Volume 1
Number 5
August 2020
Pages 929–1474

Materials Advances

rsc.li/materials-advances

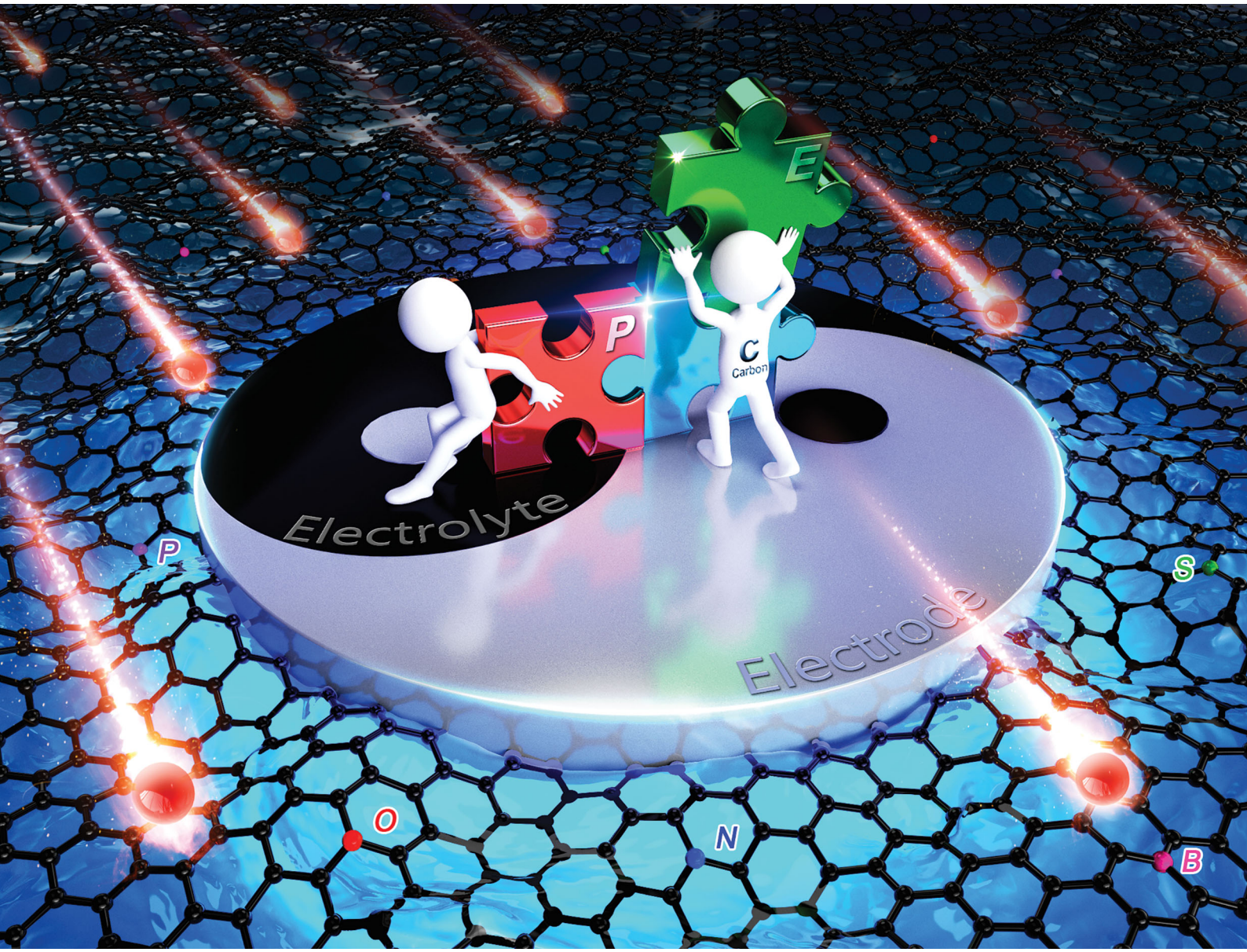

ISSN 2633-5409

ROYAL SOCIETY OF CHEMISTRY

REVIEW ARTICLE
Liangchun Li, Lihua Gan, Mingxian Liu *et al.*
Recent advances in carbon-based supercapacitors

Materials Advances

ROYAL SOCIETY OF CHEMISTRY

REVIEW

View Article Online
View Journal | View Issue

Check for updates

Cite this: *Mater. Adv.*, 2020, **1**, 945

Recent advances in carbon-based supercapacitors

Ling Miao,[a] Ziyang Song,[a] Dazhang Zhu,[a] Liangchun Li, *[a] Lihua Gan *[a] and Mingxian Liu *[ab]

Rapid advancements in modern electronics have been starved of further breakthroughs to achieve high-energy, large-power, and long-running energy storage devices. Carbon-based supercapacitors (CSs) are promising large-power systems that can store electrical energy at the interface between the carbonaceous electrode surface and adsorbed electrolyte layer. However, commercial CSs using activated carbons suffer from limited energy densities in the organic electrolytes owing to sluggish mass diffusion and restricted charge accumulation. To overcome these issues, significant efforts have been devoted toward increasing the energy storage of CSs by the exploration of both large-capacitance electrodes and high-potential electrolytes. This paper reviews the recent advances made in the two core components (*i.e.*, electrodes and electrolytes) of CSs. Firstly, we describe the involved energy storage mechanisms of CSs, followed by a brief overview of the key factors affecting the electrochemical performances. Then, novel design concepts have been summarized that can be used to fabricate carbon-based electrodes, such as microporous carbons, mesoporous carbons, hierarchical porous carbons, functionalized carbons, and carbon composites. Further, tailoring of the geometrical morphologies, pore structures, and surface functionalities can be discussed in pursuit of large-capacitance electrodes. Furthermore, various types of aqueous and nonaqueous electrolytes, such as water-in-salt, organic media, ionic liquids, and (quasi-)solid-state electrolytes, have been systematically investigated to settle the water hydrolysis concern of traditional electrolytes. Finally, the challenges in maximizing the synergistic effect between the electrodes and electrolytes are summarized, and we have proposed the future outlook for the development of advanced CSs.

Received 16th June 2020,
Accepted 5th July 2020

DOI: 10.1039/d0ma00384k

rsc.li/materials-advances

Open Access Article. Published on 07 Adooleessa 2020. Downloaded on 01/02/2026 6:27:40 PM.
This article is licensed under a Creative Commons Attribution-NonCommercial 3.0 Unported Licence.

1. Introduction

Energy conversion and storage is the fundamental pillar of modern society driven by the mutual promotion between environmental consciousness and economic development.[1] The diversification of portable electronic systems and the

[a] *Shanghai Key Lab of Chemical Assessment and Sustainability, School of Chemical Science and Engineering, Tongji University, Shanghai 200092, P. R. China. E-mail: lilc@tongji.edu.cn, ganlh@tongji.edu.cn, liumx@tongji.edu.cn*
[b] *College of Chemistry and Molecular Engineering, Zhengzhou University, Zhengzhou 450001, P. R. China*

Ling Miao

Ling Miao is a Postdoctoral Fellow in Prof. Mingxian Liu's group at Tongji University. She received her PhD from the School of Chemical Science and Engineering, Tongji University (2018). Her research interests focus on the design and tailored synthesis of ionic-liquid-derived porous carbons for energy-related applications.

Ziyang Song

Ziyang Song received his BS in 2016 from Jinggangshan University, China. He currently continues to pursue his PhD under the supervision of Prof. Mingxian Liu at Tongji University. His research currently focuses on the design and synthesis of advanced carbon materials, as well as exploring new solid gel electrolytes for energy conversion and storage.

Open Access Article. Published on 07 Adooleessa 2020. Downloaded on 01/02/2026 6:27:40 PM.
This article is licensed under a Creative Commons Attribution-NonCommercial 3.0 Unported Licence.

ongoing spread of electronics have been starved of further breakthroughs to achieve high-energy, large-power, and long-running energy storage devices.[1–3] Carbon-based supercapacitors (CSs) are promising large-power devices that keep on dominating the commercial market, affording fascinating features such as fast pulses of energy, millions of charge/discharge cycles, wide operating temperatures, and high Coulombic efficiencies.[4,5] CSs consist of two carbonaceous electrodes soaked in an aqueous/nonaqueous electrolyte, and a porous membrane separator allowing electrolyte permeation (Fig. 1). Their energy storage mechanism is fundamentally derived from reversible charge separation at each interface of the electrolyte with the cathode/anode surface to form two closely spaced charge layers.[5] The corresponding "double-layer capacitance" ($C_D = \varepsilon A/d$, where ε is the dielectric constant) arises from the minimal separation distance (d, down to a few angstroms) and large interfacial area (A) between the intrinsic double-layer configuration. Such physical interfacial contact makes CSs fully charged/discharged within seconds with large power delivery/uptake. However, commercial CSs using activated carbons suffer from limited energy densities (<10 W h kg^{-1}) in organic electrolytes owing to the sluggish mass diffusion and restricted charge accumulation.

To overcome this issue, significant efforts have been devoted toward increasing the energy storage ($E = 0.5CV^2$) of CSs by the exploration of two core components, *i.e.*, large-capacitance (C) electrodes and high-potential (V) electrolytes.[5,6] Regarding the role of carbon-based electrodes, the design of large-surface-area carbon materials with engineered surface topography/pore feature or doping defects/functionalities to optimize the electrochemical activity, surface polarization, and electrical conductivity has become intensive research realms. On the other hand, with regard to exploiting electrolytes, particularly aqueous electrolytes with wider potential windows and non-aqueous electrolytes with higher ionic conductivities, electrochemical inertness and operation safety have become highly desirable for advanced CSs. Besides, pseudocapacitors or asymmetric/hybrid capacitors are also involved in the pursuit

Dazhang Zhu

Dazhang Zhu received his PhD in Environmental Science from Tongji University (2007) and became a Professor in the School of Chemical Science and Engineering, Tongji University (2017). His research interests include the controllable preparation of nanocrystals/nanostructures and their applications in supercapacitors and environmental protection.

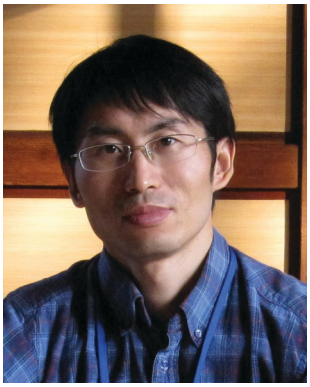

Liangchun Li

Liangchun Li received his PhD in 2009 at the Institute of Chemistry, Chinese Academy of Sciences (ICCAS), China. In 2009–2012, he was a Special Postdoctoral Researcher at RIKEN, Japan. In 2012, he joined the group of Prof. S. Kitagawa in Kyoto University. In 2013, he obtained his JSPS Fellowship. After his post doc research, he became a Professor in the School of Chemical Science and Engineering (2015), Tongji University. His current research efforts are focused on the development of porous coordination polymers for catalysts and derived porous carbons for energy storage.

Lihua Gan

Lihua Gan received his PhD in Materials Physics and Chemistry from Tongji University and became a Professor at the School of Chemical Science and Engineering in Tongji University (2005). His research interests include the design and application of nanomaterials, which cover porous metal oxides, various carbonaceous materials, and carbon-based materials. These nanomaterials are used in supercapacitors and lithium-ion batteries, and they are used as adsorbents for the treatment of pollutants.

Mingxian Liu

Mingxian Liu received his PhD in Physical Chemistry from Tongji University (2009). He started his postdoctoral research in East China University of Science and Technology (2009–2011). After that, he joined the School of Chemical Science and Engineering at Tongji University, and he became a Professor in 2016. His current research interests focus on the structural design and controllable synthesis of carbon-based materials for energy conversion and storage.

This journal is © The Royal Society of Chemistry 2020

Open Access Article. Published on 07 Adooleessa 2020. Downloaded on 01/02/2026 6:27:40 PM.
This article is licensed under a Creative Commons Attribution-NonCommercial 3.0 Unported Licence.

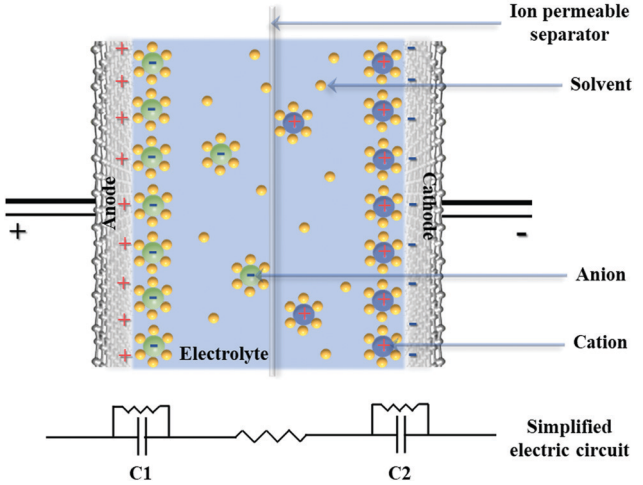

Fig. 1 Schematic representation of CSs.

of high-performance CSs: the modification of pseudo-active substances endows bare carbons with supplementary faradaic pseudocapacitance based on the electron transfer mechanism, while the hybrid of capacitive carbon and pseudocapacitive/battery-type electrode can bridge the voltage gap between the two electrodes to increase the device potential.[6,7] However, these upgraded device configurations generally come with undesired decreases in the power/cycling capabilities caused by the limited kinetics of redox reactions or phase transformation of active materials.[8] Therefore, the fundamental challenge for advanced CSs is how to maximize the role of the carbon/electrolyte in an ideal configuration to achieve high-energy, large-power, and long-running devices.

Porous carbons have been sustainably popularized as electrode materials in CSs, with the help of a representative report on anomalously increased capacitance in the subnanopores and other overwhelming theoretical/experimental studies.[9–12] Besides the common physicochemical stability and electronic properties, porous carbons stand out because of their versatile syntheses. Alternative carbon precursors encompass conventional biomasses and phenolic resins as well as novel organic salts/polymers such as metal salts, metal–organic frameworks (MOFs), covalent organic frameworks, conjugated microporous polymers, hypercrosslinked polymers, ionic liquids and poly(ionic liquid)s, *etc.*[13–16] High flexibility in the precursor choice and condition regulation can customize ideal porous carbon electrodes with the following structural superiorities: (a) large surface area to guarantee a vast accumulation platform for high energy storage, coupled with abundant adsorbing sites exposed on the surface topography to improve the accessible surface area;[17,18] (b) tunable pore structures to ensure the rapid transmission of electrolyte ions and continuous infiltration into the electrode surface, thereby enabling higher power delivery;[11,19,20] (c) surface wettability/activity to boost the electrolyte/electrode interfacial contact and afford more active sites for improved charge accumulation and ion kinetics;[21–23] and (d) stable conductive frameworks for long-term operation.[7,24,25] In the following sections, we focus on the recent advances in the two core components (*i.e.*, electrodes and electrolytes) of CSs. Novel fabrication strategies of carbon-based materials are highlighted with tailoring the geometrical morphologies, pore structures, and surface functionalities in pursuit of large-capacitance electrodes. Furthermore, a brief overview of emerging high-potential electrolytes is presented, such as water-in-salt (WIS), organic media, ionic liquids, and (quasi-)solid-state electrolytes. Finally, the challenges in realizing the electrode/electrolyte synergy are summarized, with future outlooks for the advancement of next-generation CSs.

2. Carbon-based electrodes

2.1. Large surface area

The International Union of Pure and Applied Chemistry (IUPAC) categorized pores according to their diameters into three types: micropore (<2 nm), mesopore (2–50 nm), and macropore (>50 nm).[26] The above formula of C_D states that the large surface area is a priority in achieving the large capacitance of carbon-based electrodes (large amounts of charged ions on the pore surface). Micropores perform a vital function in supplying a vast accumulation platform for high energy storage *via* molecular sieving and controlled diffusion effects.[9,17,27,28] As such, activated carbons with predominant microporosity have long been the most popular as supercapacitor electrodes. These materials are usually produced by the pre-carbonization of carbon-rich precursors (particularly biomass sources) and subsequent physical/chemical activation to afford microporous structures.[13] Physical activation is conducted in an oxidative atmosphere (*e.g.*, CO_2, O_2, or steam) at higher temperatures of 700–1200 °C, whereas chemical activation refers to heat treatment with chemicals (KOH, NaOH, H_3PO_4, $ZnCl_2$, K_2CO_3, *etc.*) at relatively lower temperatures. For instance, Wang's group prepared wrinkled porous carbon nanosheets through the carbonization and alkali activation of biomass sugarcane bagasse pith/chitosan, and the resulting typical carbon with a high surface area of 1786.1 $m^2\ g^{-1}$ exhibited electrode capacitances of 339/280 F g^{-1} at current densities of 0.25/100 A g^{-1} in 6 M KOH electrolyte.[29] In another example, Gao's group reported a dual-activator approach with egg yolk as the precursor and KOH/$C_3N_3Na_3S_3$ as the activators (Fig. 2a).[30] By regulating the mass ratio of egg yolk/$C_3N_3Na_3S_3$, as-obtained carbon materials afforded a tunable microporous area (26.26–74.69%) with the largest surface area (3519.50 $m^2\ g^{-1}$) and pore volume (2.68 $cm^3\ g^{-1}$), contributing to the maximum energy density at 12.7 W h kg^{-1} in H_2SO_4 (Fig. 2b and e).

2.2. Morphology control

Large surface area is always desirable for CSs, but the electrode capacitance does not necessarily increase along with the surface area because the entire area is not electrochemically accessible to the electrolyte ions, particularly in excess of 1500 $m^2\ g^{-1}$.[31] Creating abundant adsorbing sites exposed on the surface topography helps to relieve the barrier toward surface accessibility for improving the storage capacity.[18] Therefore, considerable research

Open Access Article. Published on 07 Adooleessa 2020. Downloaded on 01/02/2026 6:27:40 PM.
This article is licensed under a Creative Commons Attribution-NonCommercial 3.0 Unported Licence.

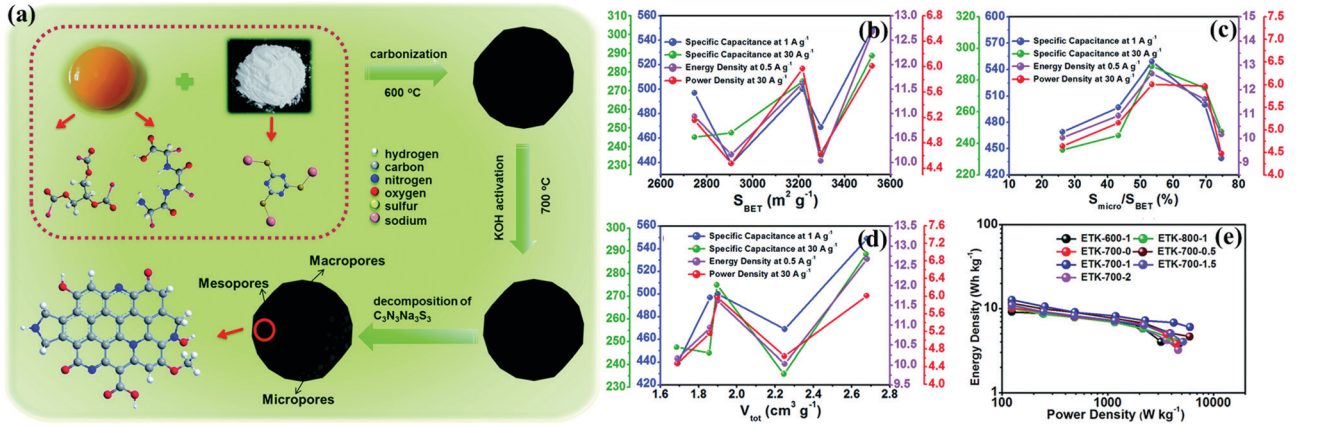

Fig. 2 Schematic of the preparation of egg yolk-derived activated carbons (a). Influence among the structural parameters, *i.e.*, S_{BET} (b); S_{micro}/S_{BET} (c); V_{tot} (d); and electrochemical performances such as specific capacitance, power density, energy density, and rate density. Ragone plots (e). (Reproduced with permission.[30] Copyright 2018, The Royal Society of Chemistry.)

efforts have focused on fabricating diverse carbon morphologies with refined control over the surface topography and interior texture.

Spherical carbon nanoarchitectures featuring the smallest surface-to-volume ratio and close-packing nature can be constructed by various synthesis methods such as emulsion polymerization, modified Stöber synthesis, self-assembly, and hydrothermal carbonization.[18,32] Recently, uniform mesoporous carbon nanospheres with large accessible pores (5–37 nm) were prepared through a versatile nanoemulsion polymerization process with dopamine as the precursor and PEO_{106}–PPO_{70}–PEO_{106} (F127) as the template in a water/ethanol system (Fig. 3a).[33] By adjusting the mediator (1,3,5-trimethylbenzene, TMB) content, the resulting

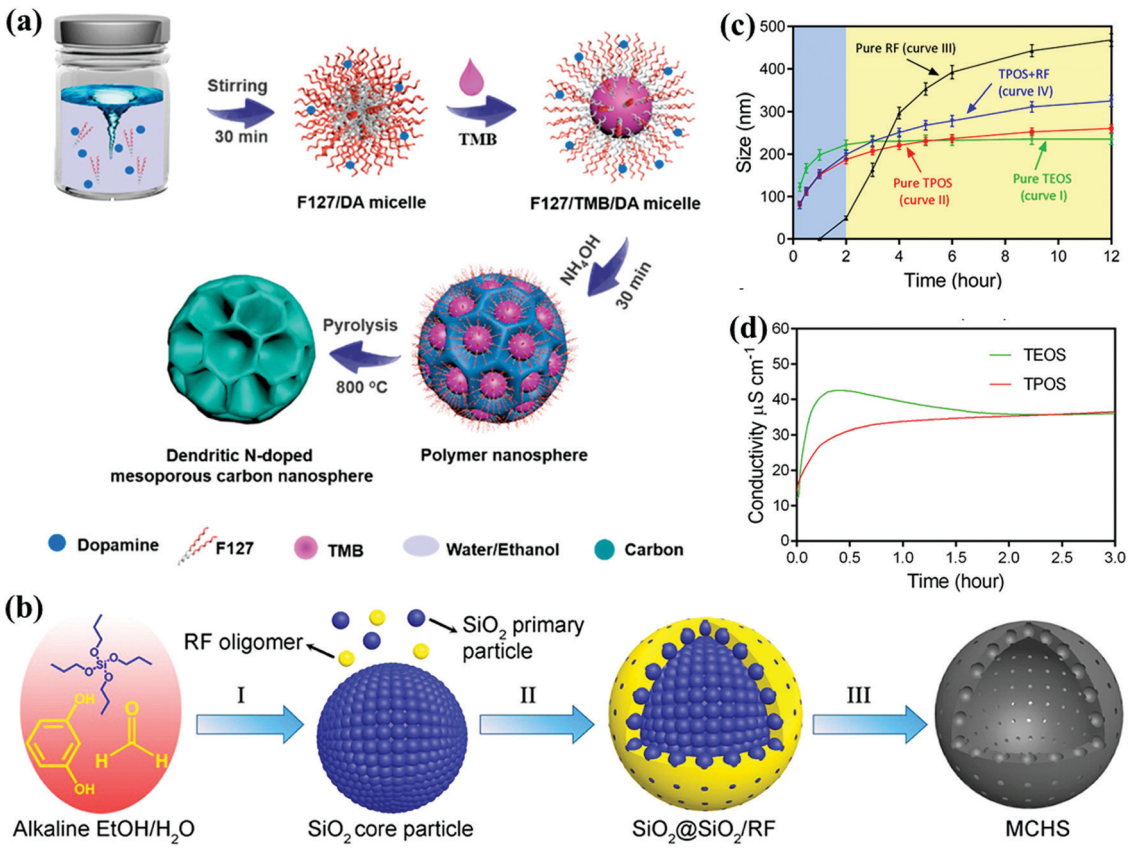

Fig. 3 Synthesis of the procedure for fabricating uniform mesoporous carbon nanospheres (a). (Reproduced with permission.[33] Copyright 2019, American Chemical Society.) Schematic of the synthesis of hollow carbon spheres (b). Particle sizes (c) and conductivity evolution (d) in TPOS/TEOS systems with reaction time. (Reproduced with permission.[34] Copyright 2016, American Chemical Society.)

 This journal is © The Royal Society of Chemistry 2020

Open Access Article. Published on 07 Adooleessa 2020. Downloaded on 01/02/2026 6:27:40 PM.
This article is licensed under a Creative Commons Attribution-NonCommercial 3.0 Unported Licence.

modification of the interfacial interactions between dopamine and F127 afforded the evolution of tunable pore diameters and various morphologies. Yu's group obtained hollow carbon spheres with controllable pore sizes (from micropores to 13.9 nm) relying on the steric effect of the propoxy of tetrapropyl orthosilicate (TPOS) using modified Stöber synthesis (Fig. 3b).[34] In contrast to traditional tetraethyl orthosilicate (TEOS), the longer hydrolysis and condensation of TPOS offered subtler monitoring ability over the SiO_2 core and oligomer formation (Fig. 3c and d), and the superior capacitive performances of 310 and 157 F g^{-1} could be realized at a current density from 1 to 50 A g^{-1} in a basic electrolyte. Further, Wei's group monitored the interfacial capillary force and polymer nanoshell thickness in the TPOS-involved Stöber process to achieve the transformation from nanoball-like architecture to carbon nanobowls with enhanced mass loading.[35] Furthermore, recently, Qiao's group designed a surfactant-assisted assembly approach to fabricate a series of multi-chamber carbon microspheres derived from 2,6-diaminopyridine.[36] A dual-surfactant system (F127 and sodium dodecylbenzenesulfonate) could induce the establishment of refined hierarchical architectures as well as tune the microsphere size in the scale of 250–3091 nm, and therefore, the as-synthesized electrode with a multi-chamber core and microporous shell functioned as a competitive supercapacitor material.

As promising supercapacitor electrodes, porous carbon nanosheets possess high aspect ratios of 2D sheet-like morphologies for short ion-transfer channels; meanwhile, their porous architectures effectively prevent the layer overlapping/restacking of the rich interfacial accessible sites.[37] Recently, the fabrication of carbon nanosheets has been performed by means of exfoliating carbon nanorods/nanotubes, lithographic patterning, chemical vapor deposition, thermal conversion, *etc.*[37–42] For example, Fischer's group developed 2D carbon nanosheets *via* the controlled pyrolysis of rod-shaped MOFs for fabricating a high-potential (1.6 V) supercapacitor (Fig. 4a).[43] Zhang's group proposed a top-down exfoliation–chlorination approach to synthesize ultrathin carbon nanosheets derived from the multilayered carbide precursor, Ti_3AlC_2.[44] The inherent 2D intersheet space in exfoliated metal carbides/nitrides (MXenes) affords graphitized carbon sheets (thickness: 3–4 nm), large accessible interface area (1766 m^2 g^{-1}), and reduced diffusion distances in the thin dimension. Besides, natural layered shrimp shells were employed as a 2D hard template to assemble graphene-like carbon nanostructures exhibiting high conductivity (7.8 S cm^{-1}) and outstanding capacitive performance of 322 F g^{-1} at 0.5 A g^{-1} in an aqueous electrolyte.[45] Recently, Qiu's group established the correlation between sheet thickness and ion transport behavior (ion diffusion coefficient and Warburg coefficient) inside the 2D carbon electrodes (Fig. 4b).[46] By using dopamine and MgAl-layered double hydroxides as the carbon suppliers and 2D structure-directing templates, carbon sheets with controllable thickness could be obtained by simply varying the reaction time, and the fabricated electrode with an optimal thickness of ~99.23 nm could be fabricated, delivering an outstanding retention rate of 81% at 100 A g^{-1} and high energy output of 94 W h kg^{-1} at 1.8 kW kg^{-1} in an ionic liquid device.

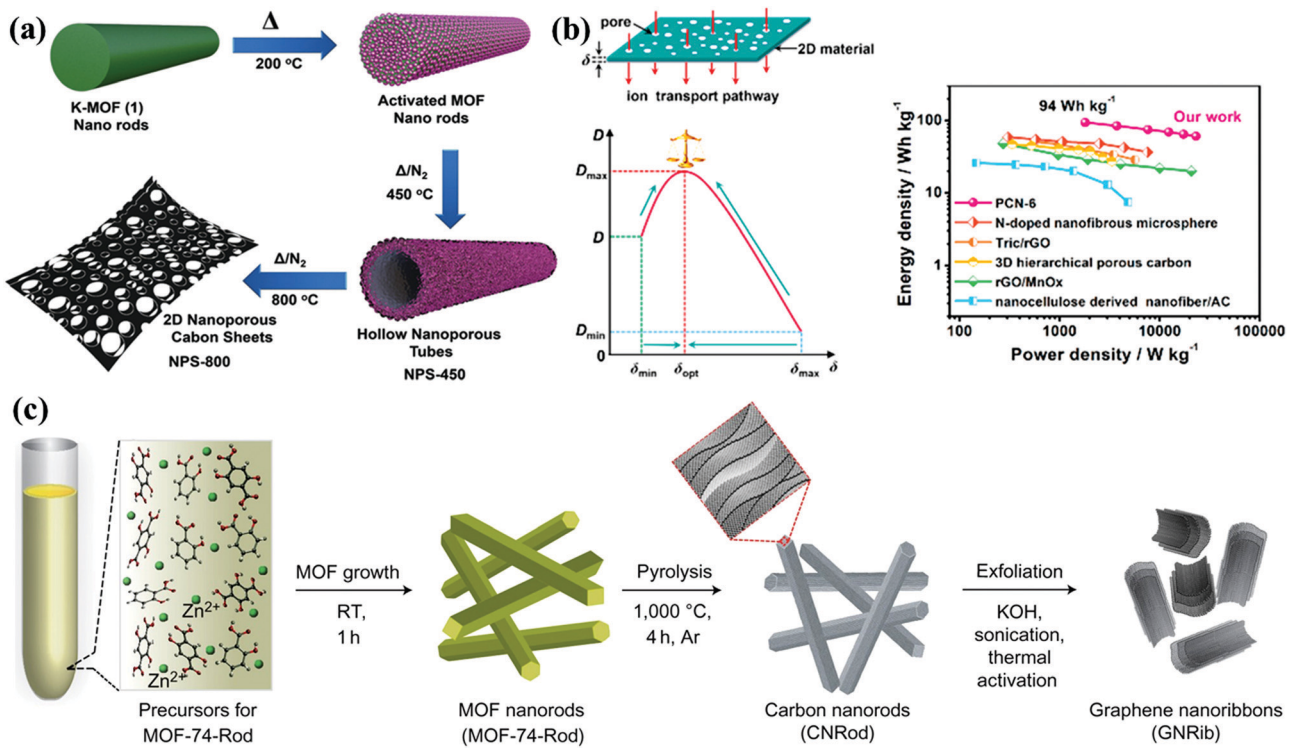

Fig. 4 Synthesis of MOF-based 2D carbon nanosheets (a). (Reproduced with permission.[43] Copyright 2018, Wiley-VCH.) Schematic illustration of ion transfer inside a 2D carbon electrode; correlation between the sheet thickness and ion transport behavior; and Ragone plots (b). (Reproduced with permission.[46] Copyright 2019, Elsevier.)

Open Access Article. Published on 07 Adooleessa 2020. Downloaded on 01/02/2026 6:27:40 PM.
This article is licensed under a Creative Commons Attribution-NonCommercial 3.0 Unported Licence.

Further, 1D carbon nanofibers and nanorods could afford shortcut channels for electron transfer, and they can be readily shaped into relevant geometries or assembled with functionalized modules for preparing advanced CSs.[47–52] For instance, Xu's group demonstrated the preparation of carbon nanorods *via* the self-sacrificial thermal conversion of rod-like MOF precursors that were prepared by the salicylic-acid-modulated hydrothermal reaction of 2,5-dihydroxyterephthalic acid and zinc nitrate, and the as-obtained carbon nanorods could be further transformed into graphene nanoribbons featuring comparable electronic properties *via* the sonication–activation treatment.[53] Zhang's group utilized the self-assembly of chitin fibers in urea/NaOH solution to fabricate unique elastic microspheres with a carbon nanofiber framework and high surface area of over 1000 $m^2\ g^{-1}$.[54] When applied as a supercapacitor electrode, this carbon material exhibited high loading intensity, distinguishing elastic recovery property (over 5 cyclic compressions at strain of 75%), and high energy delivery of 58.7 W h kg^{-1} in organic media. Chen's group synthesized a novel self-standing composite electrode (hexagonal nanoprism carbon arrays supported on carbon fiber substrates) by chemical vapor deposition using ethylenediamine precursor and ZnO sacrifice template.[55] The *in situ* growth on carbon fiber lowered the interfacial resistance for rapid electron transport, which effectively contributed toward the superior rate performance with sweep rate/current load increasing to 20 V s^{-1}/300 mA cm^{-2} in a binder-free supercapacitor.

Generally, external-templating strategies offer precise control over diverse morphologies as mentioned above, and they can be further extended to build core–shell/hollow and other complex nanoarchitectures that synergize the accessible interior spaces/active interfaces into a single system.[18,56,57] For example, Yu's group reported a new rigid-interface-induced outward contraction approach to fabricate hollow mesoporous carbon nanocubes with MOF as the precursor (Fig. 5a).[58] A thick mesoporous SiO_2 layer on MOF nanocubes could offset the inward contraction of the MOF@SiO_2 core–shell architecture at higher temperatures, and the subsequent outward contraction of the surplus frameworks induced the formation of carbon materials in the mesoporous walls and hollow cavities after template removal. Yang's group constructed a spheres-in-tube hierarchical porous nanostructure by filling anodic aluminum oxide channels with SiO_2 nanoparticles and subsequent polypyrrole coating, and the resultant carbon electrode exhibited superior capacitive performances than those of pure nanotubes/hollow spheres.[59] Alternatively, solvent-induced/template-free approaches allow the straightforward and scalable assembly of advanced carbon nanoarchitectures.[37,60–64] Feng's group reported the comprehensive construction of porous carbon superstructures *via* the hierarchical assembly of polyimide precursor sheets (Fig. 5b).[65] By changing the monomer concentrations in an aprotic solvent, the assembly of linear polymer chains could be easily monitored, yielding a class of unprecedented hierarchical superstructures such as lantern-shaped/flower-like nanospheres. Kim's group developed a Lewis acid/base-interaction-mediated self-assembly strategy on the basis of classic Friedel–Crafts crosslinking reactions to prepare functionalized carbon materials with well-engineered morphologies.[66] Layered, tubular, or hollow spherical assemblies were readily accessible *via* the rational combination between aromatic hydrocarbon monomers (base) and Lewis acid catalysts in common solvents. These inspiring findings have put forward new insights into the facile fabrication of alternative carbon nanoarchitectures, and in-depth efforts are still underway to realize fine control over the geometric parameters in solvent-induced/template-free processes.

2.3. Pore structure regulation

Appropriate regulation of pore diameters in carbon materials can be used to transport sufficient electrolyte ions throughout the electrodes, consequently allowing carbon surfaces to be fully utilized. Micropores mainly contribute toward a vast accumulation platform through molecular sieving and controlled diffusion effects as mentioned above, while meso-/macropores can shorten the transportation route and reduce the interfacial resistance of the electrolytes as ion-diffusion shortcuts to the fine micropores.[13,19] Moreover, hierarchical porous structures consisting of interconnected micro-, meso-, and

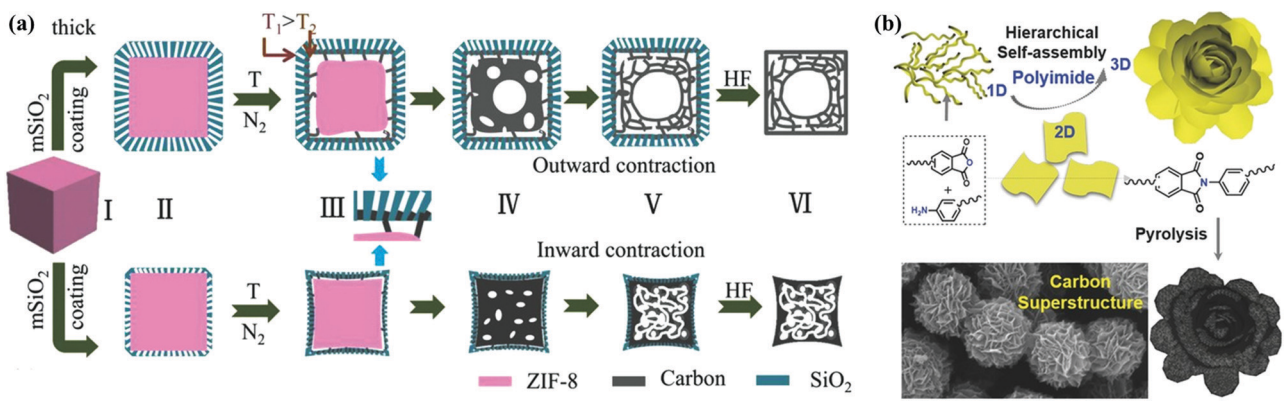

Fig. 5 Schematic illustration of hollow mesoporous carbon nanocubes (a). (Reproduced with permission.[58] Copyright 2017, Wiley-VCH.) Fabrication scheme of porous carbon superstructures (b). (Reproduced with permission.[65] Copyright 2016, Wiley-VCH.)

This journal is © The Royal Society of Chemistry 2020

Open Access Article. Published on 07 Adooleessa 2020. Downloaded on 01/02/2026 6:27:40 PM.
This article is licensed under a Creative Commons Attribution-NonCommercial 3.0 Unported Licence.

macropores are particularly interesting for high-performance CSs in consideration of the synergistic effects among the abundant micropores as ion-adsorbing sites and interconnected meso-/macropores ensuring rapid ion transmission, substantially achieving mutual enhancements in energy/power densities.[11,19,20] Furthermore, open and interconnected pore architectures accelerate continuous ion-diffusion kinetics within the pores, and they subsequently offer an easy approach to fabricate active electrode surfaces for compact devices particularly with large volumetric capacitances.[11] Therefore, considerable research efforts have been focused on developing facile and efficient fabrication methods to realize the integral regulation of controlling the pore size distribution within the carbon materials.

Activated carbons with a tiny micropore diameter (<0.5 nm) and tortuous pore alleys are not adequately accessible in commercial organic electrolytes owing to hampered or even blocked mass diffusion.[5] Tailoring the micropore diameter and shape is essential for enhanced surface accessibility, particularly in ionic liquids/organic electrolytes, to maximize the double-layer capacitances.[9,17,27,67–69] As two pioneering classes, micropore textures of zeolite-templated carbons could recently be customized according to different diameters/shapes of zeolite pores where the lanthanum-catalyzed carbonization of acetylene/ethylene occurred.[70] Chlorine treatment and physical activation of crosslinked polycarbosilane aerogels endowed the carbide-derived carbon with enlarged surface area/micropore volume (2410 $m^2\ g^{-1}$/0.63 $cm^3\ g^{-1}$) and therefore high capacitance of 170 $F\ g^{-1}$ at 0.1 $A\ g^{-1}$ in $EMIMBF_4$ and stable operation even at 60 $A\ g^{-1}$ in $TEABF_4$/ACN.[71] Beyond these, elaborately designed microporous carbons are mainly fabricated based on the similar self-porogen/template role of novel metal complexes.[72–75] Another highlighted fabrication strategy is the direct pyrolysis of emerging organic polymers (*e.g.*, covalent organic frameworks, conjugated microporous polymers, and hypercrosslinked polymers) assembled by building blocks with intrinsic microporosity and periodic skeleton.[76] Recently, Shim's group constructed a triazine-based covalent organic polymer with predominant micropores as the carbon precursor *via* the Friedel–Crafts reaction.[77] Upon further physical activation, the surface area increased to 2003 $m^2\ g^{-1}$ without sacrificing the narrow micropore diameter distribution (0.5–1.5 nm). Wang's group reported a novel hypercrosslinked polymerization route to obtain a stable microporous precursor frame as the growing polymer chains were crosslinked with adjacent rigid bridges to avoid frame mobilization/collapse (Fig. 6a).[78] As expected, the carbon electrode with well-retained micropore textures delivered a high energy density of 16.2 W h kg^{-1} at a power density of 50 W kg^{-1} and capacitance retention of 92% over 10 000 cycles (Fig. 6b and c).

Ordered mesopore paths in carbon materials can be introduced to improve the utilization of micropores since they can create express entries for electrolyte transmission into the inner electrode surface even at high currents, thereby enabling remarkable rate/power performances.[19] During the past few decades, the hard-template nanocasting method has become mature and versatile for the assembly of the required mesoporous textures.[19,79,80] The applied porous solid templates (SiO_2, MgO, Fe_3O_4, *etc.*) inversely replicated the interior structures into ultimate carbons.[81–84] For instance, Chen's group synthesized monodispersed carbon spheres with tunable mesopore size (3.1–10.0 nm) based on the self-activation calcination of phenolic resin encapsulated in the *in situ* generated silica nanoreactors from TEOS (Fig. 7a).[85] Choy's group recently proposed a cost-effective geopolymer approach to obtain an appropriate mesopore ratio in carbons, and natural clay as the silica supplier for lab-made geopolymer templates was ~400 times cheaper as compared to TEOS.[86]

With regard to direct soft-template strategies, tunable mesostructures can be generated based on the cooperative assembly between the precursor molecules and single-chain surfactants/block copolymers as sacrificial organic templates.[11,87,88] Suitable pyrolysis/extraction processes have been developed for the effective elimination of surfactant templates; nowadays, a big family of block copolymer templates such as PS–P4VP/PEO, PEO–PPO–PEO, PPO–PEO–PPO, and so on (PS: polystyrene; P4VP: poly(4-vinyl pyridine); PEO: polypropylene oxide; and PPO: polyethylene oxide)

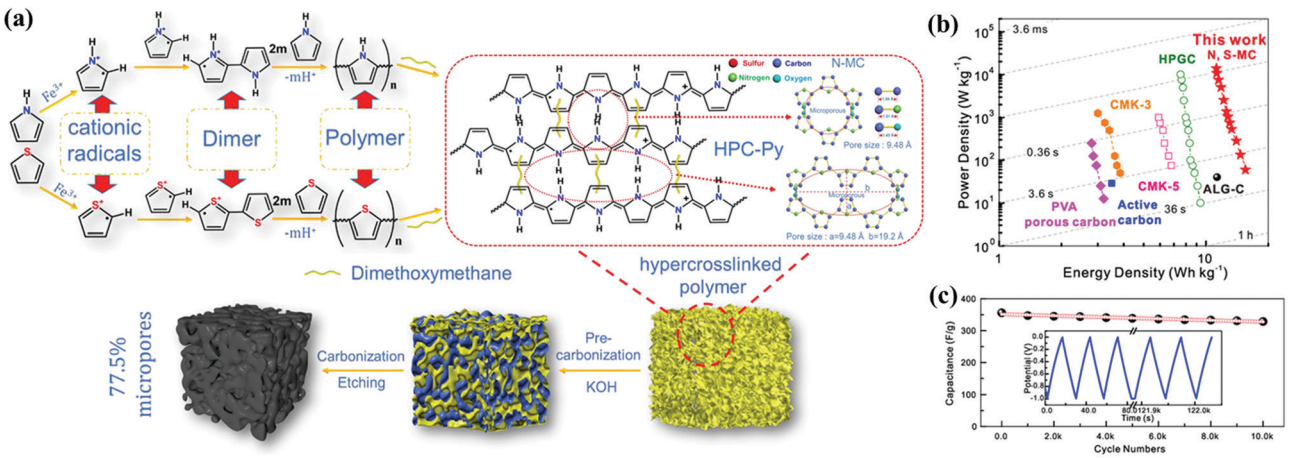

Fig. 6 Synthesis of hypercrosslinked polymer-derived carbons (a). Ragone plots (b). Long-term cycling performance (c). (Reproduced with permission.[78] Copyright 2019, Elsevier.)

Open Access Article. Published on 07 Adooleessa 2020. Downloaded on 01/02/2026 6:27:40 PM.
This article is licensed under a Creative Commons Attribution-NonCommercial 3.0 Unported Licence.

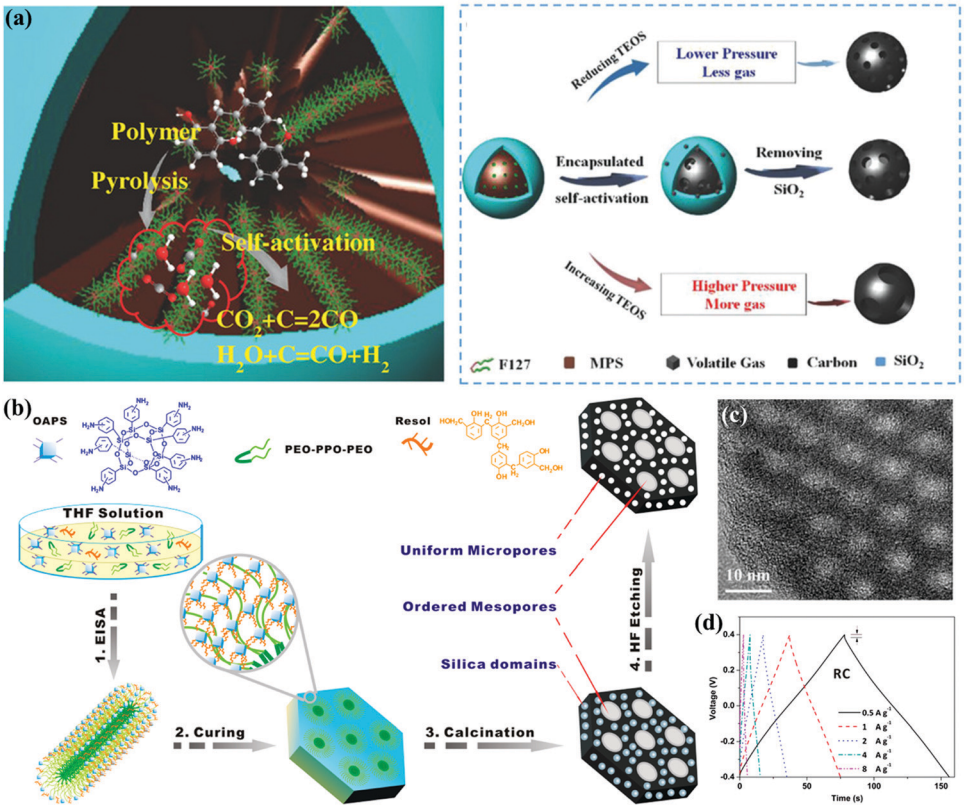

Fig. 7 Schematic illustration of monodispersed mesoporous carbon spheres (a). (Reproduced with permission.[85] Copyright 2018, Wiley-VCH.) Schematic illustration of ordered mesoporous carbons (b). TEM image (c). Galvanostatic charge/discharge curves (d). (Reproduced with permission.[98] Copyright 2016, Elsevier.)

have been successfully utilized in these strategies.[89–93] For instance, Zhang's group developed a confined self-assembly process to synthesize MXene-derived mesoporous carbon layers with phenolic resol as an additional carbon precursor in the presence of the F127 template.[94] F127 with hydrophilic PEO segments can easily interact with the precursor molecules, and similar mesopore size distributions centered at 3.1 and 7–12 nm can be obtained within the carbon materials after thermosetting at 100 °C for a rigid polymer structure and sequential two-step pyrolysis for simultaneous template removal. Gao's group prepared interconnected mesoporous carbon spheres with a large pore volume of 1.12–3.22 $cm^3\ g^{-1}$ and tunable pore size of 5–20 nm *via* a sol–gel process by regulating the volume ratio of ethanol/water and the dosage of a cationic Gemini surfactant template, *i.e.*, pentane-1,5-bis(dimethylcetyl ammonium bromide).[95] Besides, combined hard–soft templating approaches have been adopted to generate multi-model pore sizes.[96,97] As a representative example, Su's group described a block-copolymer-assisted approach based on aminophenyl-functionalized polyhedral oligosilsesquioxanes as the carbon source as well as soft template to prepare carbon electrodes with large pore volume of 1.19 $cm^3\ g^{-1}$, highly ordered mesopores (~4 nm), and uniform micropores (~1 nm) (Fig. 7b and c).[98] The unique nanostructure could be attributed to the molecule-level role of the template in the inherent siloxane cages, and the resultant electrode exhibited an outstanding rate ability with 97/94% capacitance preservation in a H_2SO_4/ionic liquid electrolyte (Fig. 7d).

Hierarchical porous carbons can be fabricated by modifying the hard-/soft-templating protocols to realize integral regulation over the pore size distribution.[16,92,99] Salt-template techniques using soluble/decomposable/reactive salts have emerged as a simple and sustainable branch of hard-templating strategies for the generation of hierarchical porosity.[16,100–102] Through this technique, certain disadvantages of other templating approaches such as the use of hazardous etchants or low-temperature restriction can be compensated, while diverse salts can interact differently with most precursor molecules during annealing when compared with SiO_2/metal oxide templates.[103] Recently, Chu's group proposed a facile and ecofriendly route from a gelatin–$NaNO_3$ biopolymer precursor to design hierarchical porous carbons with a large adsorbing surface of 2872.2 $m^2\ g^{-1}$ and mesopores/macropores centered at 2–4 and 50–150 nm, respectively (Fig. 8a).[104] The decomposition of $NaNO_3$ above 600 °C released activating gases (CO_2/N_2/O_2/NO) to yield a micro-/mesoporous structure, and vacancies/macropores formed by the water removal of Na_2O depended on the hard-templating effect of nanoconfined $NaNO_3$. Gan's group fabricated unique hollow carbon nanorods *via* the direct carbonization of an all-in-one deep-eutectic-solvent source, wherein $ZnCl_2$ was involved in the formation of the polymer shell as a raw reactant and also hydrolyzed for forming the final $ZnCl_2/Zn_2OCl_2{\cdot}2H_2O$/ZnO core.[105] The combination of micro-/mesoporous shells (thickness: 100 nm) and open hollow nanorods (width: 400 nm) within

 This journal is © The Royal Society of Chemistry 2020

Open Access Article. Published on 07 Adooleessa 2020. Downloaded on 01/02/2026 6:27:40 PM.
This article is licensed under a Creative Commons Attribution-NonCommercial 3.0 Unported Licence.

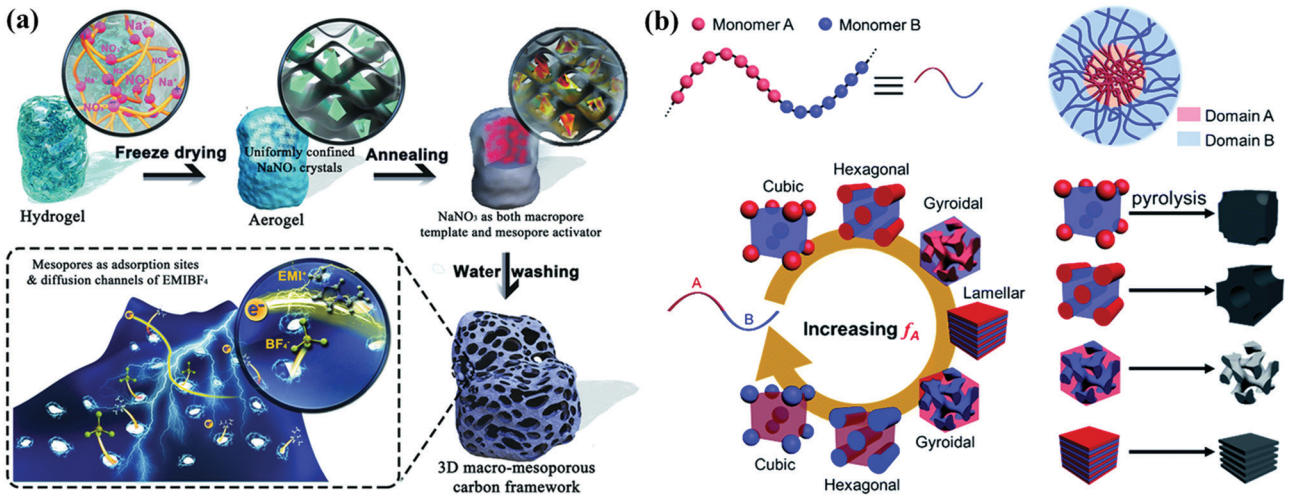

Fig. 8 Schematic illustration of the synthesis of hierarchical porous carbons from a gelatin–$NaNO_3$ biopolymer (a). (Reproduced with permission.[104] Copyright 2018, Wiley-VCH.) Examples of porous carbon structures after the calcination of block copolymers (b). (Reproduced with permission.[92] Copyright 2019, The Royal Society of Chemistry.)

the carbons endowed the ionic-liquid-based device with long-term operation at 4 V and a three-fold energy density value (116.5 W h kg^{-1}) when compared with commercial activated carbon tested under the same configuration.

With regard to modified soft-template constituents, the direct fabrication of hierarchical porous carbons from block copolymers becomes an alternate template-free strategy if the precursors consist of one polymer block with high carbon residue and the other block as the self-porogen during high-temperature calcination (Fig. 8b).[92,106–108] Chen's group recently reported a self-template approach to synthesize N-doped hierarchical porous carbons by calcining polyacrylonitrile-*block*-PS copolymers.[109] PS, as the self-template block, promoted the generation of mesopores (6–11 nm), while micropores developed by the activation of the carbon-supply block (polyacrylonitrile) contributed to a large surface area of 2104.5 cm^2 g^{-1}. Inspired by such a design concept, multiple physically interlaced polymer networks with different thermostabilities (*i.e.*, interpenetrating polymer networks) have been employed to obtain multiscale pore distributions.[110–113] Instead of covalently bonded chains, molecule-level interlaced networks tend to generate highly interconnected hierarchical porous carbon foam as the macro-phase separation between the carbon sources/pore formers can be avoided during annealing. Besides, the simultaneous carbonization–activation process was considered to be another noteworthy template-free approach for the construction of 3D interconnected macrostructures because of the high-temperature decomposition of organics in alkaline media.[114–118] As a typical example, Fan's group reported the one-step pyrolysis of KOH-assisted wheat flour to obtain interconnected honeycomb-like porous carbons.[119] The alkali-treated flour gelatin as the self-porogen could undergo a series of stages such as framework decomposition, volume expansion, and intermediate foaming during annealing to form hierarchical porous structures. The 3D interconnected honeycomb-like architecture facilitated charge transfer and storage within the carbon, demonstrating the development of a simple and cost-effective strategy for fabricating high-performance carbon electrode materials.

2.4. Heteroatom functionalization

Doping carbon materials with heteroatom (N, O, S, B, P, *etc.*) functionalities has considerably improved the electrochemical performances of carbon-based electrodes.[22,120] Firstly, binding heterogeneous atoms into the carbon backbone induces positive partial charges on the neighboring carbon atoms/heteroatoms with lower electronegativity to present a polarized electrode surface, and therefore, these polarized sites enhance the interactions with electrolyte ions to facilitate adsorption.[20,23] Secondly, the substitutive incorporation of electron-donor heteroatoms supplements the lone pair of electrons to the delocalized carbon framework for improved intrinsic conductivity, and the decreased valence band contributes toward the long-term running and high electron density at the Fermi level.[25] Thirdly, the embedment of pseudo-active heteroatoms can facilitate proton adsorption and endow bare carbons with remarkable faradaic pseudocapacitance based on electrochemical redox reactions.[22,121] Additionally, the co-/multi-doping of diverse heteroatoms probably produces synergistic contributions induced by spin/charge redistribution, consequently conducive toward affording dense electroactive density and improved overall electrode performance.[120] However, excessive/highly active heteroatoms doped by various fabrication methods and conditions could lead to undeveloped porosity or framework collapse in functionalized carbons and render CSs with decayed performances. Therefore, considerable research effort has been focused on achieving synergy between heteroatom doping and porous architecture by means of suitable fabrication methods and conditions (Table 1).

Functionalized carbons are generally fabricated by posttreatment procedures of the as-prepared carbon materials at elevated temperatures or self-doping by pyrolyzing heteroatom-rich

Open Access Article. Published on 07 Adooleessa 2020. Downloaded on 01/02/2026 6:27:40 PM.
This article is licensed under a Creative Commons Attribution-NonCommercial 3.0 Unported Licence.

Table 1 Supercapacitive performances of carbon materials as per recent studies in the literature

Material	Surface area ($m^2\ g^{-1}$)	Pore volume ($cm^3\ g^{-1}$)	Heteroatom content	Measurement system	Capacitance ($F\ g^{-1}$)	Energy density ($W\ h\ kg^{-1}$)	Power density ($W\ kg^{-1}$)	Ref.
N-doped porous carbon nanosheets	1786.1	0.8157	N: 2.10 at%, O: 7.11 at%	6 M KOH, 0.25 A g^{-1}	339	11.77	34.11	29
N/O/S-doped hierarchical porous carbon materials	3519.50	2.68	—	1 M H_2SO_4, 1 A g^{-1}	549	12.7	—	30
Mesoporous hollow carbon spheres	1582	2.45	—	6 M KOH, 1 A g^{-1}	310	—	—	34
N/S-*co*-doped carbon nanobowls	1567	2.25	N: 3.3 wt%, S: 1.7 wt%	6 M KOH, 0.1 A g^{-1}	279	9.6	25	35
N-doped multi-chamber carbon microspheres	1797	0.96	N: 4.58 wt%, O: 2.12 wt%	6 M KOH, 0.2 A g^{-1}	301	—	—	36
N-rich porous carbon nanosheets	2406	—	N: 9.4 at%, O: 4.7 at%	$EMIMBF_4$, 0.5 A g^{-1}	250	139	500	40
2D porous carbon nanosheets	1907	0.77	N: 1.54 at%, O: 6.59 at%	$EMIMBF_4$, 1 A g^{-1}	221	94	1800	46
Porous carbon nanorods	1559	—	N: 1.47 at%, O: 0.62 at%	1 M H_2SO_4, 0.05 A g^{-1}	187	—	—	53
N-doped porous carbon nanofibrous microspheres	1147	2.12	N: 2.4 at%, O: 6.1 at%	EMIMTFSI, 5 mV s^{-1}	113	58.7	300	54
Spheres-in-tube hierarchical porous carbon	318	0.78	N: 8.74 at%, O: 3.39 at%	1 M Na_2SO_4, 0.2 A g^{-1}	—	29.5	401	59
N-doped porous carbon superstructures	1375	0.996	N: 3.46 wt%, O: 7.99 wt%	6 M KOH, 0.6 A g^{-1}	~364	—	—	65
Porous interconnected carbon nanosheets	2220	1.11	—	1 M $TEABF_4$/ACN, 0.1 A g^{-1}	150	~30	13 000	72
Ultramicroporous carbon materials	1312	0.67	—	$EMIMBF_4$, 0.2 A g^{-1}	223	32.5	—	75
N/S-doped porous carbon	1339	0.96	N: 4.5 at%, S: 5.8 at%	6 M KOH, 0.2 A g^{-1}	464	16.2	50	78
Order mesoporous carbon spheres	1186	0.27	—	6 M KOH, 1 A g^{-1}	226.1	27	980	85
N-rich mesoporous carbons	458	0.42	N: 19.10 wt%	1 M H_2SO_4, 0.2 A g^{-1}	252	—	—	91
N/O-doped hierarchical porous carbon nanorods	1882	—	N: 8.1 wt%, O: 10.0 wt%	$EMIMBF_4$, 0.2 A g^{-1}	214	116.5	472	105
Honeycomb-like porous carbon foam	1313	0.716	N: 1.1 at%, O: 11.2 at%	1 M Na_2SO_4, 2 mV s^{-1}	260	29.3	—	119
B/N-codoped carbon nanosheets	2362	1.448	N: 3.1 at%, B: 0.5 at%	1 M Na_2SO_4, 0.5 A g^{-1}	235.6	30.1	225.1	124
N-doped microporous carbon spheres	1478	0.76	N: 8.71 at%, O: 7.89 at%	6 M KOH, 1 A g^{-1}	292	8.75	500	130

precursors (*e.g.*, organic salts, synthetic polymers, and biomass sources).[122] The highly praised self-doping strategy allows the homogenous distribution of heteroatoms and multispecies, but it is relatively confined to the chemical stability of reaction systems and the precursor thermostability when compared with the widely applicable posttreatment approach. With an increase in the number of comprehensive studies, the self-doping strategy has been recently subdivided into adding a supplementary dopant (*e.g.*, ethanediamine or phosphoric/boric acid) to the carbon precursors before pyrolyzing or the direct pyrolysis of organic salt/polymer precursors assembled by heteroatom-containing building blocks.[123] The supplementary dopant can not only provide plentiful heteroatoms, but also serve as a catalyst, stabilizer, activator, or structure-directing agent. For example, Jia's group synthesized chitosan-derived N/B-codoped porous carbon nanosheets with three amino acids and boric acid as the N/B source.[124] Additionally, amino acids interacted with chitosan as the structure-directing agent to induce architecture evolution, and boric acid and KOH acted as the reactive templates for creating micropores and mesopores (2–4 nm) in the final carbon. Wang's group demonstrated that the presence of poly(ionic liquid)s was beneficial for optimizing the hydrothermal carbonization of sugar precursors for N-doped porous carbon nanoparticles, wherein the poly(ionic liquid) chains introduced electrostatic repulsion for minimized particle agglomeration and unexpectedly functioned as the pore former and N supply.[125] As an extension of the post-doping strategy, the one-step doping activation is frequently applied *via* directly calcining the mixtures of carbon precursors and heteroatom-doped activators,[123] and the resultant N-rich microporous carbons activated by $NaNH_2$ afforded outstanding capacitance of 350.2 F g^{-1} at 1 A g^{-1} in 6 M KOH with excellent rate retention of 74.2% at 10 A g^{-1}.[126]

Another desirable route toward fabricating functionalized carbons at a higher doping level is the direct pyrolysis of organic salt/polymer precursors (*e.g.*, metal complexes, conjugated polymer networks, ionic liquids, and poly(ionic liquid)s).[14–16] Through the judicious assembly of molecular building blocks, heterogeneous/crosslinkable/decomposable modules can be introduced into organic salt/polymer precursors to simultaneously optimize the desired functionality/porosity. Recently, 3D hierarchical porous carbon with large interlayer space and rich

 This journal is © The Royal Society of Chemistry 2020

Open Access Article. Published on 07 Adooleessa 2020. Downloaded on 01/02/2026 6:27:40 PM.
This article is licensed under a Creative Commons Attribution-NonCommercial 3.0 Unported Licence.

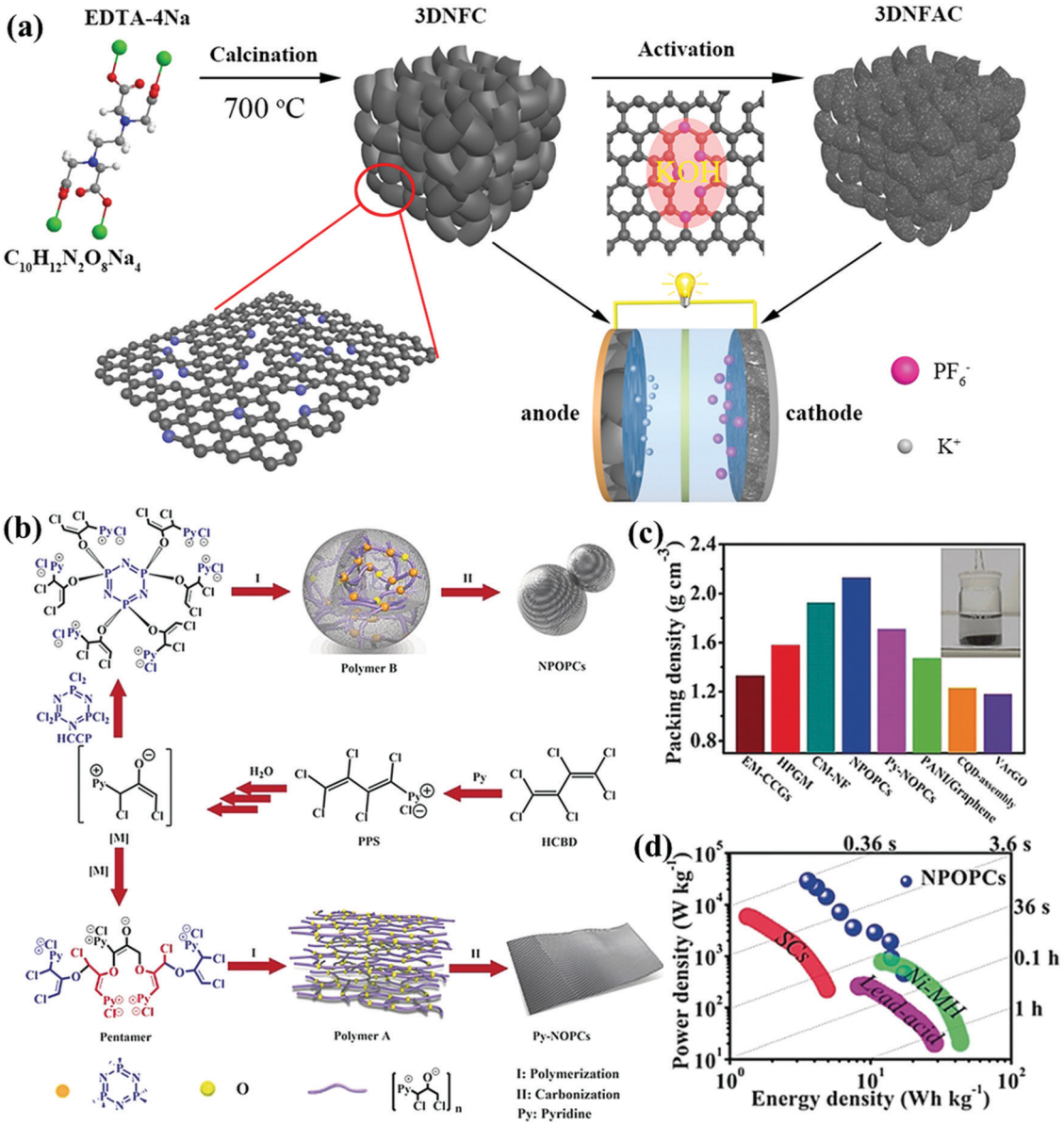

Fig. 9 Schematic illustration of N-rich 3D hierarchical porous carbons (a). (Reproduced with permission.[127] Copyright 2019, Elsevier.) Synthesis of multi-heteroatom-doped porous carbons (b). Packing density (c). Ragone plots (d). (Reproduced with permission.[133] Copyright 2019, Wiley-VCH.)

N content (5.74 at%) was fabricated by the direct calcination of tetrasodium ethylenediamine tetraacetic acid, wherein the decomposed C/N-containing skeleton of the salt precursor transformed into a N-doped carbon product coated on the self-generated Na_2CO_3 template (Fig. 9a).[127] Similarly, MOFs assembled by versatile organic ligands and metal ions enriched the possibilities for designed compositions/structures in the final products, and metal species could be used to obtain carbon composites or as a hard template for additional porosities.[14,128] Conjugated polymer networks assembled *via* the covalent bonding of multifunctional aromatic building blocks allow a wealth of choices of heteroatom incorporations with targeted locations, and the intensive inter-/intrachain π–π interactions of the robust conjugated skeleton guarantee smooth conversion into porous carbon nanoarchitectures by direct calcination.[15,65,129–132] Wang's group fabricated a novel class of multi-heteroatom-doped porous carbons based on the *in situ* dehalogenation of heteroatom-containing nucleophiles with halogenated conjugated dienes (Fig. 9b).[133] As-obtained carbons with various P/N/O and abundant multimodal pores afforded a high packing density (2.13 g cm^{-3}) and remarkable gravimetric/volumetric energy densities of 17.3 W h kg^{-1}/36.8 W h L^{-1} in an alkaline electrolyte, even approaching those of Ni-MH cells (Fig. 9c and d). Further, Liu's group developed a universal amine/benzoquinone-derived strategy to prepare high redox-active N/O-codoped porous carbons with various geometries and high surface areas to support the double-layer capacitance.[134] Moreover, the pseudocapacitive contribution of the electroactive species was well illuminated due to the fast redox reactions of quinone/hydroquinone shifts and pyrrolic/pyridinic-N responses in acid

Open Access Article. Published on 07 Adooleessa 2020. Downloaded on 01/02/2026 6:27:40 PM.
This article is licensed under a Creative Commons Attribution-NonCommercial 3.0 Unported Licence.

electrolytes, and the assembled supercapacitor afforded exceptional energy delivery of 18.2 W h kg^{-1} at 300 W kg^{-1}. Following this direction, poly(ionic liquid)s as an emerging carbon precursor class not only inherit the composition designability of the final carbons *via* matching the cations/anion pairs of monomeric ionic liquids, but also enable the flexible tuning of their structures/morphologies owing to versatile polymeric chains.[16,135] Furthermore, the poly(ionic liquid) matrix can readily crosslink the templates for targeted porous nanoarchitectures[74,136,137] or be shaped/processed *via* classical polymer operations (electrospinning, spin-coating, embossing, *etc.*) for solid-state/flexible CSs.[16,138–140]

2.5. Carbon composites

The modification of pseudo-active substances (*e.g.*, metal species and conducting polymers) endows bare carbons with supplementary pseudocapacitance based on the electron transfer mechanism.[6,7] Meanwhile, fabricating composite materials by employing carbon as the support boosts the electrochemical utilization of pseudo-active sites and simultaneously serves as efficient conductive pathways for improved electron transfer and mechanical stability.[8] Moreover, the hybrid of capacitive carbon and pseudocapacitive/battery-type electrode can bridge the voltage gap between the two electrodes to increase the device potential.[7] Therefore, considerable research efforts have been devoted toward fabricating optimal architectures to completely utilize the structural superiorities and electroactivities of each substance toward realizing competitive volumetric performances within dense composite electrodes (Table 2).

Metal-oxide-modified carbons are the characteristic surface-redox pseudocapacitive materials for symmetric and asymmetric CSs, since high capacitances could be achieved through the electrochemical reactions of electrolyte ions onto/near the active surface.[6,141–145] Shi's group prepared a free-standing MnO_2/carbon sphere/graphene electrode film by a simple vacuum filtration process and subsequent solution infiltration.[146] After modifying with high-capacitive MnO_2, the composite film delivered higher volumetric capacitance (277.8 F cm^{-3}) than that of a carbon sphere/graphene film, and correspondingly higher energy density of 25.6 W h L^{-1} coupled with capacitance retention of 94.1% over 5000 cycles in a Na_2SO_4-based symmetric supercapacitor. Yushin's group demonstrated the integration of N-doped carbon nanowires@metal oxide (MnO_2 and Fe_2O_3) composites into conductive fabrics for asymmetric supercapacitors (Fig. 10a).[147] N-doped carbon nanowires functioned as a stable conductive substrate, while the shortened diffusion channels within the metal oxide particles largely facilitated ion transportation, giving rise to high areal capacitance (72 mF cm^{-2}) for the aqueous-gel-based asymmetric device operated at 1.6 V. Metal-oxide-modified carbons can also be employed as electrode materials in ionic-liquid-based supercapacitors.[148–150] Oschatz's group reported the facile deposition of MnO_2 nanosplotches on N/S-doped mesoporous carbon matrix, and the as-obtained composite electrode exhibited outstanding electrochemical properties in an ionic liquid ($EMIMBF_4$)-based symmetric supercapacitor, *i.e.*, large capacitance (200 F g^{-1} at 2 mV s^{-1}) at 3.5 V and ultrastable cycling feature within a wide operating temperature.[148] Further theoretical calculations revealed that the high capacitance of the composite electrode could be attributed to the enhanced electrolyte adsorption and restructuring at the electrolyte/metal oxide@carbon interface, which could promote further improvements in high energy storage and broader operation applicability.

Battery–capacitor hybrid devices combine capacitive carbon and battery-type electrodes, exhibiting energy storage close to those of batteries and power output approximately that of supercapacitors.[7,151–154] Nevertheless, battery-type materials generally exhibit limited kinetics during redox reactions rooted from the sluggish phase transformation rate.[8] Wang's group synthesized and employed hierarchical porous carbon nanosheets and MnO@C nanocomposites as the positive and negative electrodes for Li-ion hybrid capacitors with kapok fiber as the precursor.[155] Nanoscale diffusion paths in the MnO@C nanocomposite facilitated Li^+ insertion/extraction and electron transfer, resulting in the improved electrochemical kinetics to balance energy delivery (100 W h kg^{-1} at 83 W kg^{-1}) and power density (20 kW kg^{-1} at 30 W h kg^{-1}) for a high-potential (4 V) device. Lee's group developed the simple fabrication of Nb_2O_5@C/rGO nanocomposite in a water-in-oil microemulsion

Table 2 Supercapacitive performances of carbon composites as per recent studies in the literature

Positive//negative material	Classification	Potential (V)	Electrolyte	Capacitance	Energy density	Power density	Ref.
Porous carbon fibers@MnO_2	Symmetric	0.8	6 M KOH	1148 F g^{-1}	10.3 W h kg^{-1}	—	141
Hierarchical porous N-doped carbon@Fe/Fe_3C	Symmetric	1.0	6 M KOH	246 F g^{-1}	—	—	142
Nanoporous duct-like graphene@MnO_2// nanoporous duct-like graphene	Asymmetric	2.0	2 M $LiNO_3$	—	28.2 mW h cm^{-3}	55.7 W cm^{-3}	143
N-doped carbon nanowires@MnO_2//N-doped carbon nanowires@Fe_2O_3	Asymmetric	1.6	5 M LiCl	72 mF cm^{-2}	—	—	147
N,S-doped mesoporous carbon@MnO_2	Symmetric	3.5	$EMIMBF_4$	200 F g^{-1}	—	—	148
Fe_2O_3@P-doped mesoporous carbon	Symmetric	3.5	$EMIMBF_4$	179 F g^{-1}	—	—	149
$Na_{0.5}MnO_2$//reduced graphene oxide@ porous carbon/Fe_3C	Hybrid	2.4	1 M Na_2SO_4	—	46.2 W h kg^{-1}	1.2 kW kg^{-1}	151
Mn_3O_4/porous carbon rods//porous carbon rods	Hybrid	4.0	1 M $LiPF_6$	—	174 W h kg^{-1}	200 W kg^{-1}	152
NiS_x@porous carbon matrix//AC	Hybrid	2.8	1 M $NaClO_4$	—	99.3 W h kg^{-1}	140 W h kg^{-1}	153
SnS/porous carbon microtubes// porous carbon microtubes	Hybrid	3.5	1 M $NaClO_4$	—	115 W h kg^{-1}	—	154
Nb_2O_5@carbon core–shell nanoparticles/ reduced graphene oxide//AC	Hybrid	3.3	1 M $NaPF_6$	—	76 W h kg^{-1}	80 W kg^{-1}	156
$FeSe_2$/N-doped carbon//AC	Hybrid	2.5	3 M KFSI	—	230 W h kg^{-1}	—	157

This journal is © The Royal Society of Chemistry 2020

Open Access Article. Published on 07 Adooleessa 2020. Downloaded on 01/02/2026 6:27:40 PM.
This article is licensed under a Creative Commons Attribution-NonCommercial 3.0 Unported Licence.

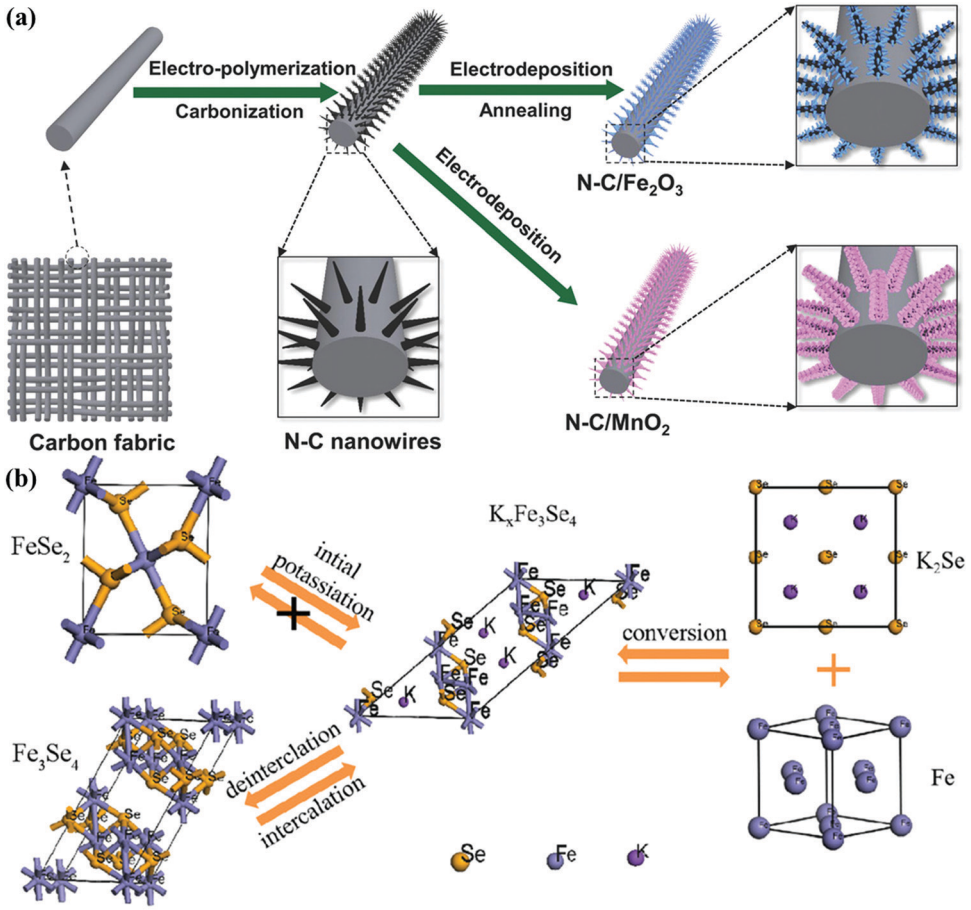

Fig. 10 Schematic of N-doped carbon nanowires@MnO_2 and N-doped carbon nanowires@Fe_2O_3 (a). (Reproduced with permission.[147] Copyright 2018, Wiley-VCH.) Schematic for the potassium storage reaction mechanism (b). (Reproduced with permission.[157] Copyright 2019, Wiley-VCH.)

assembly system for the high-power Na-ion hybrid capacitor anode.[156] The hybrid device using the Nb_2O_5@C/rGO anode and an activated carbon cathode showed high energy density of 76 W h kg^{-1} in the voltage window of 1.0–4.3 V as well as exceptional power density (20.8 kW kg^{-1}), and the stable cycling life could be attributed to the uniform Nb_2O_5@C particle deposition between the rGO layers to prevent layer restacking. Lu's group employed a simple solvothermal approach to prepare 3D N-doped carbon-coated $FeSe_2$ clusters as the anode for K-ion hybrid capacitors.[157] Carbon coating and unique 3D architecture effectively offered abundant active sites, improved conductivity, and charge transfer shortcuts, and therefore, the assembled hybrid device delivered an energy density of 230 W h kg^{-1} due to the transformation from $FeSe_2$ to Fe_3Se_4 in electrochemical reactions (Fig. 10b). The long lifetime and high power density (920 W kg^{-1}) further demonstrated the role of $FeSe_2$-modified carbons as emerging hybrid capacitor anodes.

3. Electrolytes

3.1. Traditional aqueous electrolytes

The electrolyte constituent and its stable operation potential play a key role in the double-layer formation and faradaic redox reaction to finally determine the energy storage and other parameters related to the electrochemical performance (Table 3). CSs using aqueous electrolytes (*e.g.*, KOH and H_2SO_4) exhibit high specific capacitance and rate performance due to their small ion diameter and excellent conductivity (one order of magnitude higher than those of nonaqueous media).[5,6] Unfortunately, the inherent obstacle in traditional aqueous electrolytes is their narrow operation potential window (below 1.23 V) impeded by water hydrolysis. Hydrogen/oxygen evolution occurs at the anode/cathode potential of around 0/1.23 V, respectively, which consequently threatens device configuration and electrochemical performance. One solution is utilizing the high overpotential of neutral electrolytes (*e.g.*, Na_2SO_4, Li_2SO_4, *etc.*) to reduce the H^+/OH^- availability for hydrogen/oxygen evolution reactions.[158–161] Frackowiak's group investigated neutral Li_2SO_4, Na_2SO_4, and Na_2SO_4 electrolytes in a wide concentration range (0.1–2.5 mol L^{-1}) for electrochemical capacitors, and the strong ion solvation enabled a working voltage of 2.2 V in 1 mol L^{-1} Li_2SO_4 with low capacitance decay (from 140 to 120 F g^{-1}) after 15 000 charge/discharge cycles (Fig. 11).[162] Another strategy is to introduce supplementary pseudocapacitance with redox-active pairs (*e.g.*, I^-/I_3^-, $Fe(CN)_6^{3-}/Fe(CN)_6^{4-}$, MV^{2+}/MV^+, and hydroquinone/quinone)

Open Access Article. Published on 07 Adooleessa 2020. Downloaded on 01/02/2026 6:27:40 PM.
This article is licensed under a Creative Commons Attribution-NonCommercial 3.0 Unported Licence.

as the electrolyte additives.[163–167] Fischer's group introduced KI as a redox additive into a traditional H_2SO_4 electrolyte, and the significant increase in the capacitance from 74 to 521 F g^{-1} could be ascribed to the redox processes between the active couples of $3I^-/I_3^-$, $2I_3^-/3I_2$, $2I^-/I_2$, and I_2/IO_3.[43] Additionally, the hybrid energy storage system extended the operational voltage (1.6 V) by altering the oxygen evolution potential, which afforded a novel strategy to achieve battery-grade energy and capacitor-grade power density for CSs.

3.2. WIS electrolytes

Highly concentrated aqueous electrolytes have also been used to effectively widen the operational potential window by relieving the electrolyte/carbon interphase from water availability. WIS electrolytes refer to super-concentrated salt solutions, and they have been frequently applied in energy-related applications of high-potential batteries and supercapacitors.[116,168–172] Such an exceptional high-potential feature can be attributed to two aspects:[168,173] (i) the super-concentrated salt layer creates an anion-involved Li^+ solvation shell strongly bonded by the coordination of Li^+ and water molecules outside, suppressing the possibility of water electrolysis; (ii) the dominant reduction process leads to dense LiF distribution as a solid–electrolyte interphase, kinetically avoiding endless decomposition of both water and anions. Nakanishi's group explored the performance of a WIS-electrolyte-based supercapacitor using activated carbon electrodes, and the assembled device containing 5 M lithium bis(trifluoromethanesulfonyl)imide (LiTFSI) achieved high operation potential of 2.4 V with prominent energy/power performances of 24 W h kg^{-1} at 0.48 kW kg^{-1} and 10 W h kg^{-1} at 7.6 kW kg^{-1}.[169] The low ionic conductivity is generally considered to be the main disadvantage of WIS electrolytes due to the strong coordination between Li^+ and water molecules, leading to unsatisfactory rate/power capabilities of CSs.[174–177] More recently, introducing extra ions with weak/inert interactions into the WIS electrolytes has further boosted the salt/water ratio to an unprecedented level, and these water-in-bisalt electrolytes with upgraded operational potential still maintain competitive conductivities and viscosities in contrast to typical organic electrolytes (Fig. 12).[178–182]

3.3. Organic electrolytes

Currently, most commercial CSs employ organic electrolytes ($TEABF_4$ in ACN/PC and tetraethylammonium tetrafluoroborate in acetonitrile/propylene carbonate) with stable operational potential of 2.5–2.8 V.[5,183–185] As mentioned above, nonaqueous media—free from the limitation of water hydrolysis—facilitate the fabrication of high-potential CSs. When compared with aqueous CSs, organic-electrolyte-based devices generally provide higher energy storage, even though their lower micropore accessibility and ionic conductivity lead to lower capacitances.[186–188] Sevilla's group synthesized highly microporous carbon nanosheets *via* the one-step carbonization of potassium citrate for supercapacitor electrodes, and the as-obtained electrode material exhibited capacitances of 150/120 F g^{-1} at 1/200 mV s^{-1} in 1 M $TEABF_4$/ACN-based organic device with energy/power densities of ~30 W h kg^{-1} at 13 kW kg^{-1} operated at 2.7 V.[72] The enhancement in specific capacitances can be realized when solvated ions undergo desolvation/distortion under certain potential and they are endowed with easy access to the size-matched pores.[9,69] Another disadvantage of organic media is the lower ionic conductivity (1 M $TEABF_4$/ACN: 0.06 S cm^{-1} at 25 °C) when compared with aqueous solutions (1 M H_2SO_4: 0.8 S cm^{-1}), which dramatically reduces the power performances owing to the sluggish mass diffusion.[186] The imposed confinement of electrolyte ions within the solvation shells notably decreases the diffusion coefficients of bulk TEA^+/BF_4^- and pure ACN solvent molecules by 1–2 orders of magnitude.[189] In addition, problems such as high cost, complicated cell assembly, and rising concerns of toxicity and flammability of organic solvents remain to be resolved.[190]

Table 3 Performances of CSs using various electrolytes as per recent studies in the literature

Electrolyte	Potential (V)	Electrode	Energy density (W h kg^{-1})	Power density (W kg^{-1})	Ref.
6 M KOH	1.0	N-doped porous carbon nanosheets	11.77	34.11	29
1 M H_2SO_4	1.0	O/N codoped porous carbons	18.2	300	134
1 M Na_2SO_4	1.8	B/N-codoped carbon nanosheets	30.1	225.1	124
1 M Li_2SO_4	2.2	Activated carbon	—	—	162
1 M KBr	1.9	Activated carbon	12.0	—	163
1 M Na_2SO_4 + $K_3Fe(CN)_6/K_4Fe(CN)_6$	2.0	Activated carbon	18.9	11 500	164
1 M H_2SO_4 + hydroquinone	1.0	Activated carbon	31.3	—	165
1 M KBr + $MVCl_2$	1.4	Activated carbon	~14	—	166
1 M H_2SO_4 + KI	1.6	2D nanoporous carbon sheets	89.73	533	43
5 M LiTFSI	2.4	Hierarchical porous carbon monoliths	24	480	169
8 M $NaClO_4$	2.5	Activated carbon	—	—	176
8 M LiOAc + 32 M KOAc	2.85	Activated carbon	77.9	149.1	181
1 M $TEABF_4$/ACN	2.7	Porous interconnected carbon nanosheets	~30	13 000	72
1.5 M $SBPBF_4$/PC + DMC	2.7	Activated carbon	29.6	12 500	184
$EMIMBF_4$	4.0	Cross-coupled macro–mesoporous carbon	92	1000	104
EMIMFSI	3.5	Activated carbon	42	—	198
$TMABF_4$ + $EMIMBF_4$	3.5	Mesoporous carbon materials	—	7500	203
$PI_{13}FSI$ + $PY_{14}FSI$	3.4	Activated carbon	42.5	—	205
c-P_4VPh-EMIMTFSI	4.0	Porous carbon	72	—	212

 This journal is © The Royal Society of Chemistry 2020

Open Access Article. Published on 07 Adooleessa 2020. Downloaded on 01/02/2026 6:27:40 PM.
This article is licensed under a Creative Commons Attribution-NonCommercial 3.0 Unported Licence.

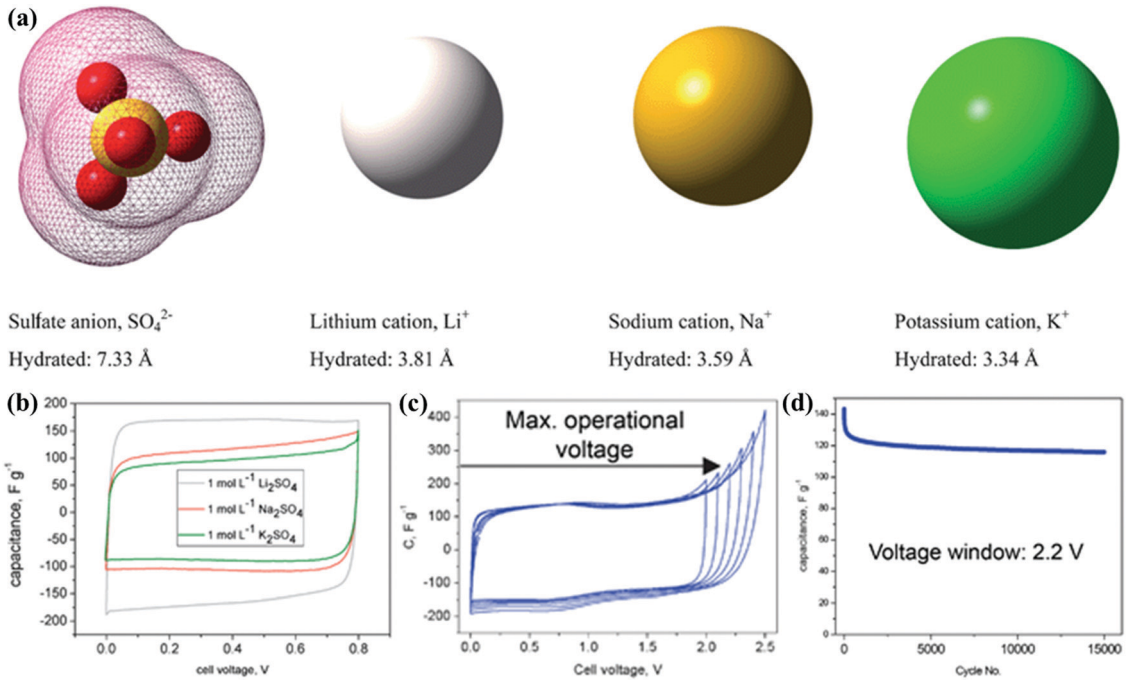

Fig. 11 Ion shapes/dimensions in aqueous solutions (a). Cyclic voltammograms in 1 mol L^{-1} Li_2SO_4/Na_2SO_4/K_2SO_4 at 1 mV s^{-1} (b) and 1 mol L^{-1} Li_2SO_4 at 10 mV s^{-1} (c). Cyclability in 1 mol L^{-1} Li_2SO_4 under 2.2 V (d). (Reproduced with permission.[162] Copyright 2012, The Royal Society of Chemistry.)

3.4. Ionic liquid electrolytes

Ionic liquids as solvent-free electrolytes have recently aroused significant interest due to their wide operation potential window (>3 V), broad temperature applicability, negligible volatility, and low flammability.[190,191] Ionic liquids are the organic salt matrix of large organic cations and inorganic/organic anions, and the highly asymmetric conjugation leads to their liquid form at room temperature or lower temperatures, consequently getting rid of additional solvent shells for charge transfer. Generally, ionic liquids explored for CS applications consist of imidazolium/pyrrolidinium/pyridinium/piperidinium/tetraalkylammonium cations coupled with anions such as Cl^-, tetrafluoroborate (BF_4^-), bis(fluorosulfonyl)imide (FSI^-), and bis(trifluoromethanesulfonyl)imide ($TFSI^-$). The physicochemical properties of ionic liquid electrolytes are strongly dependent on the choice of cation/anion couples.[192–196] Ma's group assembled ionic-liquid-based CSs with an operational potential window of 4.0 V by pairing 1-ethyl-3-methylimidazolium ($EMIM^+$) and BF_4^-/$TFSI^-$; notably, the energy/power densities in $EMIMBF_4$ and EMIMTFSI were 106.4 and 135.6 W h kg^{-1}, respectively, at a power output of 10 kW kg^{-1}.[197] Chang's group achieved optimized capacitive performances of 120/60 F g^{-1} at 0.5/10 A g^{-1} in EMIMFSI because of its low viscosity (17.9 MPa s) and rapid ion transfer, and replacing $EMIM^+$ with PMP^+ enhanced the device potential of the activated carbon-assembled supercapacitor to 3.5 V and energy delivery to 42 W h kg^{-1} at the expense of long cycling lifetime.[198] Ionic liquids can work well in a broad temperature range since their negligible and stable volatility endows them with extended fluid scope and combustion resistance.[199–201] Oschatz's group demonstrated ultrastable cycling performance (over 90% capacitance retention after 5000 cycles) of the $EMIMBF_4$-based supercapacitor operated in a broad temperature range of −20 to 60 °C, wherein the low resistance could be attributed to the low viscosity and high conductivity of the unelectrolyzed $EMIMBF_4$ at higher temperatures and its low glass transition temperature (−91 °C).[148] Grinstaff's group described the physicochemical features of a

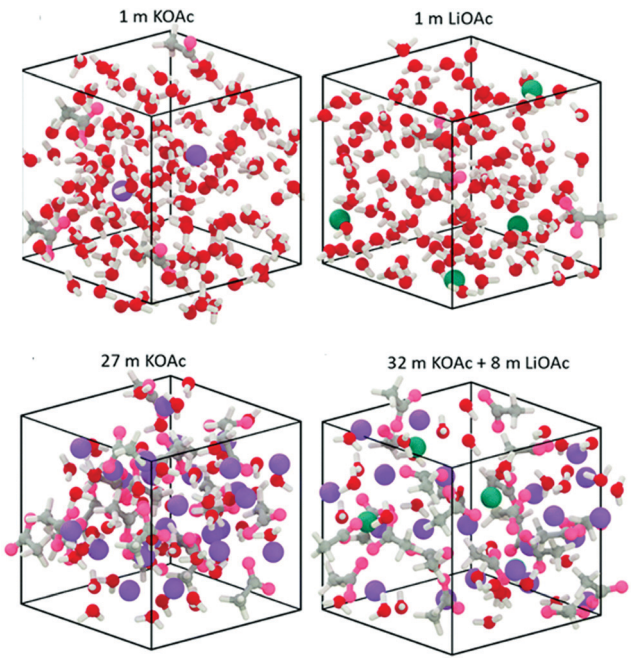

Fig. 12 Visualization of WIS and water-in-bisalt systems. (Reproduced with permission.[178] Copyright 2018, The Royal Society of Chemistry.)

Open Access Article. Published on 07 Adooleessa 2020. Downloaded on 01/02/2026 6:27:40 PM.
This article is licensed under a Creative Commons Attribution-NonCommercial 3.0 Unported Licence.

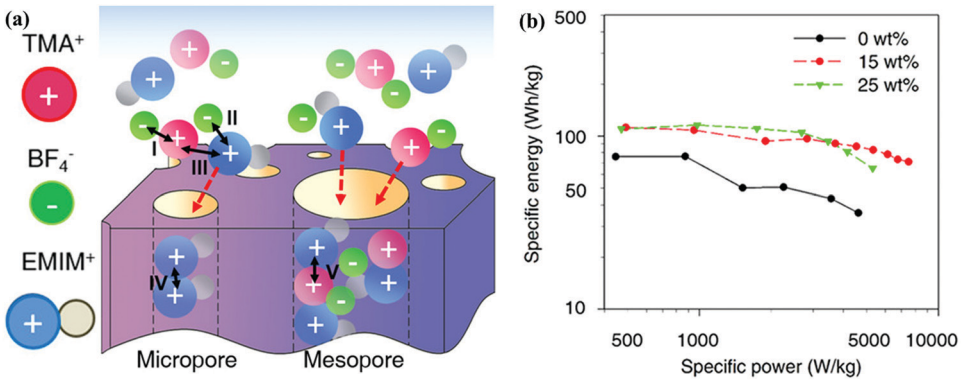

Fig. 13 Schematic of the selective charging behavior of $TMABF_4$/$EMIMBF_4$ ionic mixture electrolyte (a). Ragone plots (b). (Reproduced with permission.[203] Copyright 2017, American Chemical Society.)

class of alkyl-ether-containing piperidinium-based ionic liquid electrolytes associated with LiTFSI for use in hybrid supercapacitors. When compared with a standard LiTFSI/PC electrolyte, the piperidinium-based electrolyte showed advantageous high conductivity and it could be effectively operated for over 10 000 cycles at 100 °C, where the LiTFSI/PC-assembled device failed after 3200 charge/discharge cycles.[202] Moreover, there is still plenty of room for the modification of ionic liquid electrolytes for use in high-performance CSs. Gogotsi's group demonstrated the in-cell charging selectivity in the $TMABF_4$/$EMIMBF_4$ ionic mixture electrolyte for simultaneously improved power/energy densities.[203] Two cations (TMA^+/$EMIM^+$) with strong cationic interactions could be arranged in denser distribution at the electrode/electrolyte interface to increase the capacitance, while the selective sieving effect of TMA^+ with weaker interactions allowed fast ion dynamics in micropores without reducing the power output (Fig. 13). The modified features of ionic mixture electrolytes invite additional experimental/theoretical exploitation for comprehensive enhancements in CS performances.[204–207]

3.5. (Quasi-)solid-state electrolytes

With the growing demand for flexible and portable electronics, (quasi-)solid-state electrolytes have become popular for use in CSs as both ion-conducting media and permeable separators, and they can be divided into gel polymer electrolyte, dry polymer electrolyte, and polyelectrolyte.[6,138] Among them, liquid-phase gel polymer electrolytes are also considered to be quasi-solid-state electrolytes, and they currently dominate solid-state CS studies because of their highest ionic conductivity.[160,186,208–212] Gel polymer electrolytes consist of a polymer matrix (*e.g.*, polyvinyl alcohol (PVA)) and liquid-state electrolyte (aqueous electrolyte, organic medium, ionic liquid, *etc.*) or conducting salts dispersed in an aqueous/organic solvent. Wu's group developed a zwitterionic poly(propylsulfonate dimethylammonium propylmethacrylamide) (PPDP)–LiCl gel electrolyte by the free-radical polymerization of propylsulfonate dimethylammonium propylmethacrylamide (PDP) and physically mixing with LiCl.[213] This PPDP–LiCl hydrogel electrolyte afforded synergy between liquid preservation capacity and ion transfer pathways; subsequently, the PPDP–LiCl-based solid-state supercapacitor exhibited a higher energy density (41.78 W h L^{-1}) than that of a PVA–LiCl-based one (26.89 W h L^{-1}) (Fig. 14). MacFarlane's group proposed a novel preparation approach for self-supported ionic liquid gel membranes by incorporating two ionogels [EMIM][NTf_2]/[C_4mpyr][eFAP] into the poly(vinylidene fluoride-*co*-hexafluoropropylene) polymer matrix.[214] The [EMIM][NTf2]-ionogel-membrane-based symmetric supercapacitor could achieve capacitances of 153/101 F g^{-1} at 0.1/10 A g^{-1}, and the flexible CS still retained specific capacitance of 119 F g^{-1} at 1 A g^{-1}. Dry polymer electrolytes consist of a polymeric network (*e.g.*, PEO) and conducting salt (LiCl, $LiClO_4$, *etc.*) without any aqueous/organic solvents.[186,215,216]

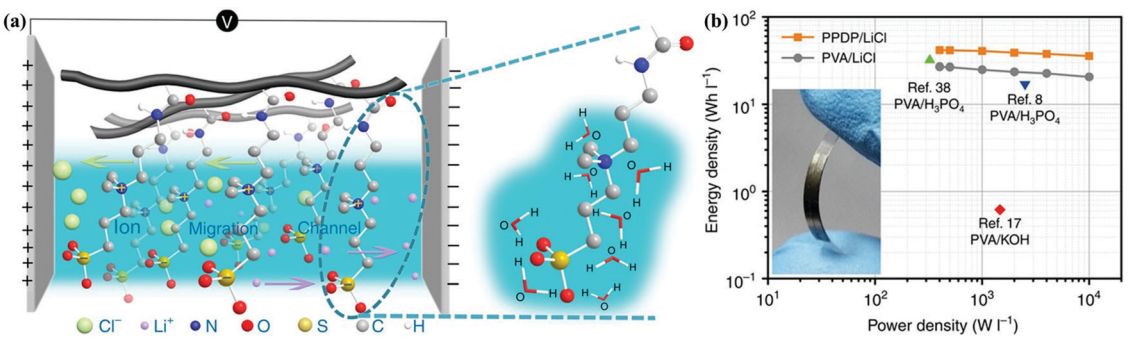

Fig. 14 Zwitterionic PPDP under an external electric field (a). Ragone plots (b). (Reproduced with permission.[213] Copyright 2016, Springer Nature.)

This journal is © The Royal Society of Chemistry 2020

Open Access Article. Published on 07 Adooleessa 2020. Downloaded on 01/02/2026 6:27:40 PM.
This article is licensed under a Creative Commons Attribution-NonCommercial 3.0 Unported Licence.

As an example of polyelectrolytes, Zhi's group fabricated a self-healable and stretchable polyelectrolyte *via* the dual crosslinking of polyacrylic acid by H-bond and vinyl hybrid SiO_2, and the corresponding polyelectrolyte-based CS delivered superior functions when compared with that offered by PVA-based acidic devices.[217] (Quasi-)solid-state electrolytes can simplify the assembling/packaging manufacture of CSs, and they can also prevent the potential leakage of liquid-state electrolytes.[3] Nevertheless, issues related to ionic conductivity (10^{-8}–10^{-5} S cm^{-1}), mechanical strength, electrochemical stability, and interfacial contact in CS applications still remain to be fully addressed for flexible and portable devices.

4. Summary and outlook

CSs are promising large-power systems that have dominated the commercial market and they offer fascinating features such as fast pulses of energy and millions of charge/discharge cycles. Porous carbons have long been the most popular electrode material due to their versatile syntheses as well as physicochemical stability and electronic properties. To meet the growing demand for energy storage, significant efforts have been devoted toward exploring large-capacitance carbon-based electrodes and high-potential electrolytes for advanced CSs. In this review, recent advances made in both the core components of CSs have been summarized. For the role of carbon-based electrodes, novel synthesis strategies of large-surface-area carbon materials with morphology control, pore structure regulation, heteroatom functionalization, and metal composite, have been highlighted in pursuit of large-capacitance electrodes. Furthermore, with regard to exploiting electrolytes, WIS and ionic-liquid-based electrolytes with wider potential windows, broader temperature applicability, or higher electrochemical inertness and operation safety, have emerged as the new trend to settle the concern regarding water hydrolysis in traditional media. Despite the significant progresses made in the development of advanced CSs in recent years, some in-depth efforts are still underway and future research directions are suggested to focus on the following:

(1) One strategy is maximizing the capacitances of carbon-based electrodes by a facile fabrication strategy to achieve synergy among the surface area, geometrical morphology, pore structure, and pseudocapacitive activity. Instead of external templating or random functionalization, self-templating and doping syntheses based on the direct pyrolysis of organic salt/polymer precursors (*e.g.*, metal complexes, conjugated polymer networks, ionic liquids, and poly(ionic liquid)s) have become in considerable demand as straightforward and cost-effective strategies for fabricating pseudo-active hierarchical porous carbons. Through the judicious assembly of molecular building blocks, pseudo-active functionalities can be doped *in situ* into the precursor skeletons; meanwhile, the multifunctional reactants serve as the self-porogen that may undergo a series of stages such as framework decomposition, filler etching/expansion, and intermediate foaming during annealing, affording micro-, meso-, and macroporous structures. Besides, in-depth correlation between the precursor chemistry and carbon architecture should be established for the task-specific fabrication of carbon-based electrodes at the molecular level by quantifying the morphological growth with solvent/precursor solubility parameters, tracking the network polymerization/crosslinking degree, speculating the possible pyrolysis mechanism, *etc.* Moreover, molecular dynamics studies and simulations help to clarify the energy storage mechanisms in carbon architectures and consequently provide the guidelines for maximizing the electrode capacitance in a certain electrolyte.

(2) Another strategy is modifying high-potential electrolytes in terms of water-in-bisalt media and ionic mixtures. The exploitation of high-potential electrolytes is a long-sought-after target shared with battery applications. When compared with traditional media, emerging WIS and ionic-liquid-based electrolytes possess overwhelming superiorities such as wider potential windows, applicability at distinct temperatures, higher electrochemical inertness, and operational safety. The physicochemical properties of electrolytes are strongly dependent on the cation/anion couples and ion concentrations of conducting salts as well as those of water or organic solvents. Introducing additional conducting salts into such super-ion-concentrated aqueous/non-aqueous systems can further elevate the energy density to a higher level, even realizing comprehensive enhancements in energy/power performances. Apart from salt mixtures, solvent mixtures have also been recently developed to modify salt solvent systems for improved ion dynamics and reduced electrolyte viscosity for comprehensively enhanced energy/power densities. Besides, ionic liquids or poly(ionic liquid)s trapped in polymer matrixes appear to resolve the leakage crisis of existing energy storage cells, and they hold a position as potential gel polymer electrolytes for flexible and portable supercapacitors.

(3) Lastly, the carbon/electrolyte compatibility can be optimized for ideal device configurations. The fundamental energy storage mechanism of CSs can be derived from fast and reversible ion adsorption at the carbon/electrolyte interfaces. Future studies should attempt to enhance interface accessibility, particularly in high-potential electrolytes by optimizing the carbon/electrolyte compatibility, including tailoring the micropore diameter/shape to accommodate larger electrolyte ions, introducing mesopore/macropore paths to transfer viscous media, and doping pseudo-active sites to enhance the interfacial interactions. With regard to upgraded device configurations, the carbon/electrolyte compatibility still remains to be optimized for relieving the limited ion kinetics/interfacial contact of redox reactions and phase transformation for hybrid/solid-state CSs. Despite these challenges in maximizing the carbon/electrolyte synergy, we believe that high-energy, large-power, and long-running CSs can be realized in the near future for ongoing commercial applications of electronics and other multipurpose fields.

Conflicts of interest

The authors declare no conflict of interest.

Open Access Article. Published on 07 Adooleessa 2020. Downloaded on 01/02/2026 6:27:40 PM.
This article is licensed under a Creative Commons Attribution-NonCommercial 3.0 Unported Licence.

Acknowledgements

This work is financially supported by the National Natural Science Foundation of China (No. 21875165, 51772216 and 21905207), the Science and Technology Commission of Shanghai Municipality, China (14DZ2261100), the Fundamental Research Funds for the Central Universities, and the Recruitment Program of Global Experts of China.

Notes and references

1 E. Pomerantseva, F. Bonaccorso, X. Feng, Y. Cui and Y. Gogotsi, *Science*, 2019, **366**, eaan8285.
2 X. Zeng, Y. Xu, Y. Yin, X. Wu, J. Yue and Y. Guo, *Mater. Today Nano*, 2019, **8**, 100057.
3 T. Lv, M. Liu, D. Zhu, L. Gan and T. Chen, *Adv. Mater.*, 2018, **30**, 1705489.
4 X. Chen, R. Paul and L. Dai, *Nat. Sci. Rev.*, 2017, **4**, 453–489.
5 P. Simon and Y. Gogotsi, *Acc. Chem. Res.*, 2012, **46**, 1094–1103.
6 Y. Wang, Y. Song and Y. Xia, *Chem. Soc. Rev.*, 2016, **45**, 5925–5950.
7 D. Tie, S. Huang, J. Wang, J. Ma, J. Zhang and Y. Zhao, *Energy Storage Mater.*, 2019, **21**, 22–40.
8 M. Lukatskaya, B. Dunn and Y. Gogotsi, *Nat. Commun.*, 2016, **7**, 12647.
9 J. Chmiola, G. Yushin, Y. Gogotsi, C. Portet, P. Simon and P.-L. Taberna, *Science*, 2006, **313**, 1760–1763.
10 P. Wu, J. Huang, V. Meunier, B. Sumpter and R. Qiao, *ACS Nano*, 2011, **5**, 9044–9051.
11 M. Benzigar, S. Talapaneni, S. Joseph, K. Ramadass, G. Singh, J. Scaranto, U. Ravon, K. Al-Bahily and A. Vinu, *Chem. Soc. Rev.*, 2018, **47**, 2680–2721.
12 W. Tian, H. Zhang, X. Duan, H. Sun, G. Shao and S. Wang, *Adv. Funct. Mater.*, 2020, **30**, 1909265.
13 S. Dutta, A. Bhaumik and C. W. Wu, *Energy Environ. Sci.*, 2014, **7**, 3574–3592.
14 B. Bhadra, A. Vinu, C. Serre and S. Jhung, *Mater. Today*, 2019, **25**, 88–111.
15 F. Xu, D. Wu, R. Fu and B. Wei, *Mater. Today*, 2017, **20**, 629–656.
16 T. P. Fellinger, A. Thomas, J. Yuan and M. Antonietti, *Adv. Mater.*, 2013, **25**, 5838–5854.
17 C. Largeot, C. Portet, J. Chmiola, P.-L. Taberna, Y. Gogotsi and P. Simon, *J. Am. Chem. Soc.*, 2008, **130**, 2730–2731.
18 P. Qiu, B. Ma, C. Hung, W. Li and D. Zhao, *Acc. Chem. Res.*, 2019, **52**, 2928–2938.
19 Y. Zhai, Y. Dou, D. Zhao, P. F. Fulvio, R. T. Mayes and S. Dai, *Adv. Mater.*, 2011, **23**, 4828–4850.
20 R. Yan, M. Antonietti and M. Oschatz, *Adv. Energy Mater.*, 2018, **8**, 1800026.
21 B. Qiu, C. Pan, W. Qian, Y. Peng, L. Qiu and F. Yan, *J. Mater. Chem. A*, 2013, **1**, 6373–6378.
22 M. Yang and Z. Zhou, *Adv. Sci.*, 2017, **4**, 1600408.
23 C. Cui, Y. Gao, J. Li, C. Yang, M. Liu, H. Jin, Z. Xia, L. Dai, Y. Lei, J. Wang and S. Wang, *Angew. Chem., Int. Ed.*, 2020, **59**, 2–8.
24 D. Puthusseri, V. Aravindan, S. Madhavi and S. Ogale, *Energy Environ. Sci.*, 2014, **7**, 728–735.
25 J. Chen, Y. Han, X. Kong, X. Deng, H. J. Park, Y. Guo, S. Jin, Z. Qi, Z. Lee and Z. Qiao, *Angew. Chem., Int. Ed.*, 2016, **55**, 13822–13827.
26 K. Sing, D. Everett, R. Haul, L. Moscou, R. Pierotti, J. Rouquérol and T. Siemieniewska, *Pure Appl. Chem.*, 1985, **57**, 603–619.
27 J. Chmiola, C. Largeot, P.-L. Taberna, P. Simon and Y. Gogotsi, *Angew. Chem., Int. Ed.*, 2008, **47**, 3392–3395.
28 X. Yang, C. Cheng, Y. Wang, L. Qiu and D. Li, *Science*, 2013, **341**, 534–537.
29 Q. Niu, K. Gao, Q. Tang, L. Wang, L. Han, H. Fang, Y. Zhang, S. Wang and L. Wang, *Carbon*, 2017, **123**, 290–298.
30 H. Xu, C. Wu, X. Wei and S. Gao, *J. Mater. Chem. A*, 2018, **6**, 15340–15347.
31 O. Barbieri, M. Hahn, A. Herzog and R. Kotz, *Carbon*, 2005, **43**, 1303–1310.
32 J. Liu, N. Wickramaratne, S. Qiao and M. Jaroniec, *Nat. Mater.*, 2015, **14**, 763–774.
33 L. Peng, C. Hung, S. Wang, X. Zhang, X. Zhu, Z. Zhao, C. Wang, Y. Tang, W. Li and D. Zhao, *J. Am. Chem. Soc.*, 2019, **141**, 7073–7080.
34 H. Zhang, O. Noonan, X. Huang, Y. Yang, C. Xu, L. Zhou and C. Yu, *ACS Nano*, 2016, **10**, 4579–4586.
35 J. Wang, H. Liu, X. Zhang, M. Shao and B. Wei, *J. Mater. Chem. A*, 2018, **6**, 17653–17661.
36 T. Wang, Y. Sun, L. Zhang, K. Li, Y. Yi, S. Song, M. Li, Z. Qiao and S. Dai, *Adv. Mater.*, 2019, **31**, 1807876.
37 Y. He, X. Zhuang, C. Lei, L. Lei, Y. Hou, Y. Mai and X. Feng, *Nano Today*, 2019, **24**, 103–119.
38 J. Gong, H. Lin, M. Antonietti and J. Yuan, *J. Mater. Chem. A*, 2016, **4**, 7313–7321.
39 H. Lyu, J. Zhu, B. Zhou, H. Cao, J. Duan, L. Chen, W. Jin and Q. Xu, *Carbon*, 2018, **139**, 740–749.
40 L. Yao, Q. Wu, P. Zhang, J. Zhang, D. Wang, Y. Li, X. Ren, H. Mi, L. Deng and Z. Zheng, *Adv. Mater.*, 2018, **30**, 1706054.
41 L. Miao, D. Zhu, M. Liu, H. Duan, Z. Wang, Y. Lv, W. Xiong, Q. Zhu, L. Li and X. Chai, *Chem. Eng. J.*, 2018, **347**, 233–242.
42 G. Yuan, Y. Liang, H. Hu, H. Li, Y. Xiao, H. Dong, Y. Liu and M. Zheng, *ACS Appl. Mater. Interfaces*, 2019, **11**, 26946–26955.
43 K. Jayaramulu, D. P. Dubal, B. Nagar, V. Ranc, O. Tomanec, M. Petr, K. K. R. Datta, R. Zboril, P. Gómez-Romero and R. A. Fischer, *Adv. Mater.*, 2018, **30**, 1705789.
44 B. Ding, J. Wang, Y. Wang, Z. Chang, G. Pang, H. Dou and X. Zhang, *Nanoscale*, 2016, **8**, 11136–11142.
45 W. Tian, Q. Gao, L. Zhang, C. Yang, Z. Li, Y. Tan, W. Qian and Z. Hang, *J. Mater. Chem. A*, 2016, **4**, 8690–8699.
46 J. Yu, C. Yu, W. Guo, Z. Wang, S. Li, J. Chang, X. Tan, Y. Ding, M. Zhang and L. Yang, *Nano Energy*, 2019, **64**, 103921.
47 G. Zhou, L. Xu, G. Hu, L. Mai and Y. Cui, *Chem. Rev.*, 2019, **119**, 11042–11109.
48 S. Li, X. Song, X. Wang, C. Xu, Y. Cao, Z. Xiao, C. Qi, M. Wu, Z. Yang, L. Fu, X. Ma and J. Gao, *Carbon*, 2020, **160**, 176–187.

 This journal is © The Royal Society of Chemistry 2020

Open Access Article. Published on 07 Adooleessa 2020. Downloaded on 01/02/2026 6:27:40 PM.
This article is licensed under a Creative Commons Attribution-NonCommercial 3.0 Unported Licence.

49 P. Shang, J. Zhang, W. Tang, Q. Xu and S. Guo, *Adv. Funct. Mater.*, 2016, **26**, 7766–7774.
50 X. Wang, Z. Na, D. Yin, C. Wang, G. Huang and L. Wang, *Energy Storage Mater.*, 2018, **12**, 103–109.
51 L. Miao, D. Zhu, M. Liu, H. Duan, Z. Wang, Y. Lv, W. Xiong, Q. Zhu, L. Li and X. Chai, *Electrochim. Acta*, 2018, **274**, 378–388.
52 D. Zhu, K. Cheng, Y. Wang, D. Sun, L. Gan, T. Chen, J. Jiang and M. Liu, *Electrochim. Acta*, 2017, **224**, 17–24.
53 P. Pachfule, D. Shinde, M. Majumder and Q. Xu, *Nat. Chem.*, 2016, **8**, 718–724.
54 D. Bo, G. Xiang, Y. Xu, F. Yan, H. Liang, J. Zhou and L. Zhang, *Nano Energy*, 2016, **27**, 482–491.
55 S. He, C. Zhang, C. Du, C. Cheng and W. Chen, *J. Power Sources*, 2019, **434**, 226701.
56 L. Wang, T. Wei, L. Sheng, L. Jiang, X. Wu, Q. Zhou, B. Yuan, J. Yue, Z. Liu and Z. Fan, *Nano Energy*, 2016, **30**, 84–92.
57 L. Jiang, J. Wang, X. Mao, X. Xu, B. Zhang, J. Yang, Y. Wang, J. Zhu and S. Hou, *Carbon*, 2017, **111**, 207–214.
58 C. Liu, X. Huang, J. Wang, H. Song, Y. Yang, Y. Liu, J. Li, L. Wang and C. Yu, *Adv. Funct. Mater.*, 2018, **28**, 1705253.
59 Z. Chen, S. Ye, S. Evans, Y. Ge, Z. Zhu, Y. Tu and X. Yang, *Small*, 2018, **14**, 1704015.
60 S. Chen, D. M. Koshy, Y. Tsao, R. Pfattner, X. Yan, D. Feng and Z. Bao, *J. Am. Chem. Soc.*, 2018, **140**, 10297–10304.
61 M. Liu, J. Qian, Y. Zhao, D. Zhu, L. Gan and L. Chen, *J. Mater. Chem. A*, 2015, **3**, 11517–11526.
62 L. Miao, D. Zhu, Y. Zhao, M. Liu, H. Duan, W. Xiong, Q. Zhu, L. Li, Y. Lv and L. Gan, *Microporous Mesoporous Mater.*, 2017, **253**, 1–9.
63 D. Qiu, J. Guan, M. Li, C. Kang, J. Wei, Y. Li, Z. Xie, F. Wang and R. Yang, *Adv. Funct. Mater.*, 2019, **29**, 1903496.
64 X. Qian, L. Miao, J. Jiang, G. Ping, W. Xiong, Y. Lv, Y. Liu, L. Gan, D. Zhu and M. Liu, *Chem. Eng. J.*, 2020, **388**, 124208.
65 Z. Xu, X. Zhuang, C. Yang, J. Cao, Z. Yao, Y. Tang, J. Jiang, D. Wu and X. Feng, *Adv. Mater.*, 2016, **28**, 1981–1987.
66 W. Song, Y. Zhang, A. Varyambath and I. Kim, *ACS Nano*, 2019, **13**, 11753–11769.
67 H. Itoi, H. Nishihara, T. Kogure and T. Kyotani, *J. Am. Chem. Soc.*, 2011, **133**, 1165–1167.
68 W. Lu, M. Liu, L. Miao, D. Zhu, X. Wang, H. Duan, Z. Wang, L. Li, Z. Xu and L. Gan, *Electrochim. Acta*, 2016, **205**, 132–141.
69 N. Jäckel, P. Simon, Y. Gogotsi and V. Presser, *ACS Energy Lett.*, 2016, **1**, 1262–1265.
70 K. Kim, T. Lee, Y. Kwon, Y. Seo, J. Song, J. K. Park, H. Lee, J. Y. Park, H. Ihee, S. J. Cho and R. Ryoo, *Nature*, 2016, **535**, 131–135.
71 M. Oschatz, S. Boukhalfa, W. Nickel, J. P. Hofmann, C. Fischer, G. Yushin and S. Kaskel, *Carbon*, 2017, **113**, 283–291.
72 M. Sevilla and A. Fuertes, *ACS Nano*, 2014, **8**, 5069–5078.
73 W. Li, S. Hu, X. Luo, Z. Li, X. Sun, M. Li, F. Liu and Y. Yu, *Adv. Mater.*, 2017, **29**, 1605820.
74 L. Miao, H. Duan, Z. Wang, Y. Lv, W. Xiong, D. Zhu, L. Gan, L. Li and M. Liu, *Chem. Eng. J.*, 2020, **382**, 122945.
75 J. Zhou, Z. Li, W. Xing, H. Shen, X. Bi, T. Zhu, Z. Qiu and S. Zhuo, *Adv. Funct. Mater.*, 2016, **26**, 7955–7964.
76 L. Borchardt, Q.-L. Zhu, M. E. Casco, R. Berger, X. Zhuang, S. Kaskel, X. Feng and Q. Xu, *Mater. Today*, 2017, **20**, 592–610.
77 M. Kim, P. Puthiaraj, Y. Qian, Y. Kim, S. Jang, S. Hwang, E. Na, W.-S. Ahn and S. E. Shim, *Electrochim. Acta*, 2018, **284**, 98–107.
78 Y. Lu, J. Liang, S. Deng, Q. He, S. Deng, Y. Hu and D. Wang, *Nano Energy*, 2019, **65**, 103993.
79 T. Kyotani, N. Sonobe and A. Tomita, *Nature*, 1988, **331**, 331–333.
80 R. Ryoo, S. H. Joo and S. Jun, *J. Phys. Chem. B*, 1999, **103**, 7743–7746.
81 Y. Fang, Y. Lv, F. Gong, Z. Wu, X. Li, H. Zhu, L. Zhou, C. Yao, F. Zhang and G. Zheng, *J. Am. Chem. Soc.*, 2015, **137**, 2808–2811.
82 Z. Song, L. Li, D. Zhu, L. Miao, H. Duan, Z. Wang, W. Xiong, Y. Lv, M. Liu and L. Gan, *J. Mater. Chem. A*, 2019, **7**, 816–826.
83 Y. Bu, T. Sun, Y. Cai, L. Du, O. Zhuo, L. Yang, Q. Wu, X. Wang and Z. Hu, *Adv. Mater.*, 2017, **29**, 1700470.
84 L. Estevez, V. Prabhakaran, A. L. Garcia, Y. Shin, J. Tao, A. M. Schwarz, J. Darsell, P. Bhattacharya, V. Shutthanandan and J.-G. Zhang, *ACS Nano*, 2017, **11**, 11047–11055.
85 J. Du, L. Liu, Z. Hu, Y. Yu, Y. Qin and A. Chen, *Adv. Funct. Mater.*, 2018, **28**, 1802332.
86 Y. Pei, G. Choi, S. Asahina, J. Yang, A. Vinu and J. Choy, *Chem. Commun.*, 2019, **55**, 3266–3269.
87 C. Liang, K. Hong, G. Guiochon, J. Mays and S. Dai, *Angew. Chem. Int. Ed.*, 2004, **43**, 5785–5789.
88 Y. Wan, Y. Shi and D. Zhao, *Chem. Mater.*, 2008, **20**, 932–945.
89 J. Tang, J. Liu, C. Li, Y. Li, M. Tade, S. Dai and Y. Yamauchi, *Angew. Chem., Int. Ed.*, 2015, **54**, 588–593.
90 J. Chen, J. Xu, S. Zhou, N. Zhao and C. Wong, *Nano Energy*, 2016, **25**, 193–202.
91 Y. Liu, Z. Wang, W. Teng, H. Zhu, J. Wang, A. Elzatahry, D. Al-Dahyan, W. Li, Y. Deng and D. Zhao, *J. Mater. Chem. A*, 2018, **6**, 3162–3170.
92 T. Liu and G. Liu, *J. Mater. Chem. A*, 2019, **7**, 23476–23488.
93 H. Peng, B. Yao, X. Wei, T. Liu, T. Kou, P. Xiao, Y. Zhang and Y. Li, *Adv. Energy Mater.*, 2019, **9**, 1803665.
94 J. Wang, J. Tang, B. Ding, V. Malgras, Z. Chang, X. Hao, Y. Wang, H. Dou, X. Zhang and Y. Yamauchi, *Nat. Commun.*, 2017, **8**, 15717.
95 W. Li, B. Li, M. Shen, Q. Gao and J. Hou, *Chem. Eng. J.*, 2020, **384**, 123309.
96 Y. Song, J. Yang, K. Wang, S. Haller, Y. Wang, C. Wang and Y. Xia, *Carbon*, 2016, **96**, 955–964.
97 Z. Qiang, Y. Xia, X. Xia and B. D. Vogt, *Chem. Mater.*, 2017, **29**, 10178–10186.
98 D. Liu, G. Cheng, H. Zhao, C. Zeng, D. Qu, L. Xiao, H. Tang, Z. Deng, Y. Li and B. Su, *Nano Energy*, 2016, **22**, 255–268.

Open Access Article. Published on 07 Adooleessa 2020. Downloaded on 01/02/2026 6:27:40 PM.
This article is licensed under a Creative Commons Attribution-NonCommercial 3.0 Unported Licence.

99 T. Liu, F. Zhang, Y. Song and Y. Li, *J. Mater. Chem. A*, 2017, **5**, 17705–17733.
100 Y. Kim, J. Park and J. Lee, *Carbon*, 2018, **126**, 215–224.
101 B. Zhang, C. Song, C. Liu, J. Min, J. Azadmanjiri, Y. Ni, R. Niu, J. Gong, Q. Zhao and T. Tang, *J. Mater. Chem. A*, 2019, **7**, 22912–22923.
102 D. Xue, D. Zhu, M. Liu, H. Duan, L. Li, X. Chai, Z. Wang, Y. Lv, W. Xiong and L. Gan, *ACS Appl. Nano Mater.*, 2018, **1**, 4998–5007.
103 N. Fechler, T. P. Fellinger and M. Antonietti, *Adv. Mater.*, 2013, **25**, 75–79.
104 J. Li, N. Wang, J. Tian, W. Qian and W. Chu, *Adv. Funct. Mater.*, 2018, **28**, 1806153.
105 D. Xue, D. Zhu, H. Duan, Z. Wang, Y. Lv, W. Xiong, L. Li, M. Liu and L. Gan, *Chem. Commun.*, 2019, **55**, 11219–11222.
106 J. M. Serrano, T. Liu, A. U. Khan, B. Botset, B. J. Stovall, Z. Xu, D. Guo, K. Cao, X. Hao, S. Cheng and G. Liu, *Chem. Mater.*, 2019, **31**, 8898–8907.
107 K. Yan, L. Kong, Y. Dai, M. Shi, K. Shen, B. Hu, Y. Luo and L. Kang, *J. Mater. Chem. A*, 2015, **3**, 22781–22793.
108 J. Yang, G. Li, M. Cai, P. Pan, Z. Li, Y. Bao and Z. Chen, *Chem. Commun.*, 2017, **53**, 5028–5031.
109 Y. Tong, X. Li, L. Xie, F. Su, J. Li, G. Sun, Y. Gao, N. Zhang, Q. Wei and C. Chen, *Energy Storage Mater.*, 2016, **3**, 140–148.
110 L. Miao, X. Qian, D. Zhu, T. Chen, G. Ping, Y. Lv, W. Xiong, Y. Liu, L. Gan and M. Liu, *Chin. Chem. Lett.*, 2019, **30**, 1445–1449.
111 D. Zhu, Y. Wang, W. Lu, H. Zhang, Z. Song, D. Luo, L. Gan, M. Liu and D. Sun, *Carbon*, 2018, **111**, 667–674.
112 J. Zhang, X. Zhong, H. Chen, Y. Gao and H. Li, *Electrochim. Acta*, 2014, **148**, 203–210.
113 B. Hu, W. B. Zhang, K. Yan, T. Zhang, K. Li, X. W. Chen, L. Kang and L. B. Kong, *RSC Adv.*, 2018, **8**, 35083–35093.
114 J. Yin, W. Zhang, N. A. Alhebshi, N. Salah and H. N. Alshareef, *Small Methods*, 2020, **4**, 1900853.
115 Y. Zhao, M. Lu, P. Tao, Y. Zhang, X. Gong, Z. Yang, G. Zhang and H. Li, *J. Power Sources*, 2016, **307**, 391–400.
116 Z. Song, H. Duan, D. Zhu, Y. Lv, W. Xiong, T. Cao, L. Li, M. Liu and L. Gan, *J. Mater. Chem. A*, 2019, **7**, 15801–15811.
117 D. Xue, D. Zhu, W. Xiong, T. Cao, Z. Wang, Y. Lv, L. Li, M. Liu and L. Gan, *ACS Sustainable Chem. Eng.*, 2019, **7**, 7024–7034.
118 G. Zhang, L. Wang, Y. Hao, X. Jin, Y. Xu, Y. Kuang, L. Dai and X. Sun, *Adv. Funct. Mater.*, 2016, **26**, 3340–3348.
119 X. Wu, L. Jiang, C. Long and Z. Fan, *Nano Energy*, 2015, **13**, 527–536.
120 J. P. Paraknowitsch and A. Thomas, *Energy Environ. Sci.*, 2013, **6**, 2839–2855.
121 T. Lin, I.-W. Chen, F. Liu, C. Yang, H. Bi, F. Xu and F. Huang, *Science*, 2015, **350**, 1508–1513.
122 Y. Deng, Y. Xie, K. Zou and X. Ji, *J. Mater. Chem. A*, 2016, **4**, 1144–1173.
123 M. Perovic, Q. Qin and M. Oschatz, *Adv. Funct. Mater.*, 2020, 1908371.
124 L. Yang, D. Wu, T. Wang and D. Jia, *ACS Appl. Mater. Interfaces*, 2020, **12**, 18692–18704.
125 P. Zhang, J. Yuan, T. P. Fellinger, M. Antonietti, H. Li and Y. Wang, *Angew. Chem., Int. Ed.*, 2013, **52**, 6028–6032.
126 Y. Zhang, L. Liu, P. Zhang, J. Wang, M. Xu, Q. Deng, Z. Zeng and S. Deng, *Chem. Eng. J.*, 2019, **355**, 309–319.
127 B. Yang, J. Chen, L. Liu, P. Ma, B. Liu, J. Lang, Y. Tang and X. Yan, *Energy Storage Mater.*, 2019, **23**, 522–529.
128 J. Hwang, R. Yan, M. Oschatz and B. V. K. J. Schmidt, *J. Mater. Chem. A*, 2018, **6**, 23521–23530.
129 H. Li, J. Li, A. Thomas and Y. Liao, *Adv. Funct. Mater.*, 2019, **29**, 1904785.
130 D. Zhu, J. Jiang, D. Sun, X. Qian, Y. Wang, L. Li, Z. Wang, X. Chai, L. Gan and M. Liu, *J. Mater. Chem. A*, 2018, **6**, 12334–12343.
131 Z. Zhou, X. Zhang, L. Xing, J. Liu, A. Kong and Y. Shan, *Electrochim. Acta*, 2019, **298**, 210–218.
132 Y. He, Z. Cheng, H. Zuo, C. Yan and Y. Liao, *ChemElectroChem*, 2020, **7**, 959–966.
133 H. Jin, X. Feng, J. Li, M. Li, Y. Xia, Y. Yuan, C. Yang, B. Dai, Z. Lin and J. Wang, *Angew. Chem. Int. Ed.*, 2019, **58**, 2397–2401.
134 Z. Song, L. Miao, L. Li, D. Zhu, Y. Lv, W. Xiong, H. Duan, Z. Wang, L. Gan and M. Liu, *J. Mater. Chem. A*, 2020, **8**, 3717–3725.
135 S. Zhang, K. Dokko and M. Watanabe, *Mater. Horiz.*, 2015, **2**, 168–197.
136 H. Li, C. J. Zhang, Y. Yan, K. Hu, X. Q. Shi, N. Wang, H. J. Lin, K. Rui, J. X. Zhu and W. Huang, *J. Power Sources*, 2020, **449**, 22750.
137 L. Miao, H. Duan, M. Liu, W. Lu, D. Zhu, T. Chen, L. Li and L. Gan, *Chem. Eng. J.*, 2017, **317**, 651–659.
138 W. Qian, J. Texter and F. Yan, *Chem. Soc. Rev.*, 2017, **46**, 1124–1159.
139 W. Zhang, S. Wei, Y. Wu, Y.-L. Wang, M. Zhang, D. Roy, H. Wang, J. Yuan and Q. Zhao, *ACS Nano*, 2019, **13**, 10261–10271.
140 J. Gong, M. Antonietti and J. Yuan, *Angew. Chem., Int. Ed.*, 2017, **56**, 7557–7563.
141 T. Liu, Z. Zhou, Y. Guo, D. Guo and G. Liu, *Nat. Commun.*, 2019, **10**, 675.
142 G. Li, J. Zhang, W. Li, K. Fan and C. Xu, *Nanoscale*, 2018, **10**, 9252–9260.
143 K. Qin, E. Liu, J. Li, J. Kang, C. Shi, C. He, F. He and N. Zhao, *Adv. Energy Mater.*, 2016, **6**, 1600755.
144 M. Liu, M. Shi, W. Lu, D. Zhu, L. Li and L. Gan, *Chem. Eng. J.*, 2017, **313**, 518–526.
145 M. Liu, X. Wang, D. Zhu, L. Li, H. Duan, Z. Xu, Z. Wang and L. Gan, *Chem. Eng. J.*, 2016, **308**, 240–247.
146 Y. Liu, X. Cai, B. Luo, M. Yan, J. Jiang and W. Shi, *Carbon*, 2016, **107**, 426–432.
147 W. Fu, E. Zhao, X. Ren, A. Magasinski and G. Yushin, *Adv. Energy Mater.*, 2018, **8**, 1703454.
148 F. Lai, J. Feng, R. Yan, G. C. Wang, M. Antonietti and M. Oschatz, *Adv. Funct. Mater.*, 2018, **28**, 1801298.
149 F. Lai, J. Feng, T. Heil, G. Wang, P. Adler, M. Antonietti and M. Oschatz, *Energy Storage Mater.*, 2019, **20**, 188–195.
150 H. Cheng, J. Meng, G. Wu and S. Chen, *Angew. Chem., Int. Ed.*, 2019, **58**, 17465–17473.

 This journal is © The Royal Society of Chemistry 2020

Open Access Article. Published on 07 Adooleessa 2020. Downloaded on 01/02/2026 6:27:40 PM.
This article is licensed under a Creative Commons Attribution-NonCommercial 3.0 Unported Licence.

151 Q. Tan, X. Chen, H. Wan, B. Zhang, X. Liu, L. Li, C. Wang, Y. Gan, P. Liang, Y. Wang, J. Zhang, H. Wang, L. Miao, J. Jiang, P. A. van Aken and H. Wang, *J. Power Sources*, 2020, **448**, 227403.
152 R. Wang, P. Liu, J. Lang, L. Zhang and X. Yan, *Energy Storage Mater.*, 2017, **6**, 53–60.
153 S. Li, W. He, B. Liu, J. Cui, X. Wang, D. Peng, B. Liu and B. Qu, *Energy Storage Mater.*, 2020, **25**, 636–643.
154 J. Zhao, G. Wang, R. Hu, K. Zhu, K. Cheng, K. Ye, D. Cao and Z. Fan, *J. Mater. Chem. A*, 2019, **7**, 4047–4054.
155 Y. Zhao, Y. Cui, J. Shi, W. Liu, Z. Shi, S. Chen, X. Wang and H. Wang, *J. Mater. Chem. A*, 2017, **5**, 15243–15252.
156 E. Lim, C. Jo, M. S. Kim, M.-H. Kim, J. Chun, H. Kim, J. Park, K. C. Roh, K. Kang, S. Yoon and J. Lee, *Adv. Funct. Mater.*, 2016, **26**, 3711–3719.
157 J. Ge, B. Wang, J. Wang, Q. Zhang and B. Lu, *Adv. Energy Mater.*, 2020, **10**, 1903277.
158 M. Yu, D. Lin, H. Feng, Y. Zeng, Y. Tong and X. Lu, *Angew. Chem., Int. Ed.*, 2017, **56**, 5454–5459.
159 J. C. Icaza and R. K. Guduru, *J. Power Sources*, 2016, **336**, 360–366.
160 N. Batisse and E. Raymundo-Piñero, *J. Power Sources*, 2017, **348**, 168–174.
161 Z. Zhou, L. Miao, H. Duan, Z. Wang, Y. Lv, W. Xiong, D. Zhu, L. Li, M. Liu and L. Gan, *Chin. Chem. Lett.*, 2020, **31**, 1226–1230.
162 K. Fic, G. Lota, M. Meller and E. Frackowiak, *Energy Environ. Sci.*, 2012, **5**, 5842–5850.
163 Q. Li, M. Haque, V. Kuzmenko, N. Ramani, P. Lundgren, A. D. Smith and P. Enoksson, *J. Power Sources*, 2017, **348**, 219–228.
164 J. Y. Hwang, M. Li, M. F. El-Kady and R. B. Kaner, *Adv. Funct. Mater.*, 2017, **27**, 1605745.
165 S. Roldán, C. Blanco, M. Granda, R. Menéndez and R. Santamaría, *Angew. Chem., Int. Ed.*, 2011, **50**, 1699–1701.
166 S. Chun, B. Evanko, X. Wang, D. Vonlanthen, X. Ji, G. D. Stucky and S. W. Boettcher, *Nat. Commun.*, 2015, **6**, 7818.
167 J. Y. Hwang, M. F. El-Kady, M. Li, C. Lin, M. Kowal, X. Han and R. B. Kaner, *Nano Today*, 2017, **15**, 15–25.
168 L. Suo, O. Borodin, T. Gao, M. Olguin, J. Ho, X. Fan, C. Luo, C. Wang and K. Xu, *Science*, 2015, **350**, 938–943.
169 G. Hasegawa, K. Kanamori, T. Kiyomura, H. Kurata, T. Abe and K. Nakanishi, *Chem. Mater.*, 2016, **28**, 3944–3950.
170 Y. Yamada, K. Usui, K. Sodeyama, S. Ko, Y. Tateyama and A. Yamada, *Nat. Energy*, 2016, **1**, 16129.
171 Q. Dou, S. Lei, D.-W. Wang, Q. Zhang, D. Xiao, H. Guo, A. Wang, H. Yang, Y. Li and S. Shi, *Energy Environ. Sci.*, 2018, **11**, 3212–3219.
172 M. Ma, Z. Shi, Y. Li, Y. Yang, Y. Zhang, Y. Wu, H. Zhao and E. Xie, *J. Mater. Chem. A*, 2020, **8**, 4827–4835.
173 N. Dubouis, P. Lemaire, B. Mirvaux, E. Salager, M. Deschamps and A. Grimaud, *Energy Environ. Sci.*, 2018, **11**, 3491–3499.
174 H. Avireddy, B. W. Byles, D. Pinto, J. M. Delgado Galindo, J. J. Biendicho, X. Wang, C. Flox, O. Crosnier, T. Brousse, E. Pomerantseva, J. R. Morante and Y. Gogotsi, *Nano Energy*, 2019, **64**, 103961.
175 D. Xiao, Q. Dou, L. Zhang, Y. Ma, S. Shi, S. Lei, H. Yu and X. Yan, *Adv. Funct. Mater.*, 2019, **29**, 1904136.
176 Q. Dou, Y. Lu, L. Su, X. Zhang, S. Lei, X. Bu, L. Liu, D. Xiao, J. Chen, S. Shi and X. Yan, *Energy Storage Mater.*, 2019, **23**, 603–609.
177 J. Yan, D. Zhu, Y. Lv, W. Xiong, M. Liu and L. Gan, *Chin. Chem. Lett.*, 2020, **31**, 579–582.
178 M. R. Lukatskaya, J. I. Feldblyum, D. G. Mackanic, F. Lissel, D. L. Michels, Y. Cui and Z. Bao, *Energy Environ. Sci.*, 2018, **11**, 2876–2883.
179 L. Suo, O. Borodin, W. Sun, X. Fan, C. Yang, F. Wang, T. Gao, Z. Ma, M. Schroeder, A. von Cresce, S. M. Russell, M. Armand, A. Angell, K. Xu and C. Wang, *Angew. Chem., Int. Ed.*, 2016, **55**, 7136–7141.
180 C. Yang, J. Chen, X. Ji, T. P. Pollard, X. Lü, C.-J. Sun, S. Hou, Q. Liu, C. Liu, T. Qing, Y. Wang, O. Borodin, Y. Ren, K. Xu and C. Wang, *Nature*, 2019, **569**, 245–250.
181 W. Deng, X. Wang, C. Liu, C. Li, J. Chen, N. Zhu, R. Li and M. Xue, *Energy Storage Mater.*, 2019, **20**, 373–379.
182 L. Chen, J. Zhang, Q. Li, J. Vatamanu, X. Ji, T. P. Pollard, C. Cui, S. Hou, J. Chen, C. Yang, L. Ma, M. S. Ding, M. Garaga, S. Greenbaum, H.-S. Lee, O. Borodin, K. Xu and C. Wang, *ACS Energy Lett.*, 2020, **5**, 968–974.
183 N. Jung, S. Kwon, D. Lee, D. Yoon, Y. Park, A. Benayad, J. Choi and J. Park, *Adv. Mater.*, 2013, **25**, 6854–6858.
184 Z. Shi, X. Yu, J. Wang, H. Hu and C. Wu, *Electrochim. Acta*, 2015, **174**, 215–220.
185 X. Yu, D. Ruan, C. Wu, J. Wang and Z. Shi, *J. Power Sources*, 2014, **265**, 309–316.
186 C. Zhong, Y. Deng, W. Hu, J. Qiao, L. Zhang and J. Zhang, *Chem. Soc. Rev.*, 2015, **44**, 7484–7539.
187 Y. Xu, Z. Lin, X. Zhong, X. Huang, N. O. Weiss, Y. Huang and X. Duan, *Nat. Commun.*, 2014, **5**, 4554.
188 K. Nomura, H. Nishihara, N. Kobayashi, T. Asada and T. Kyotani, *Energy Environ. Sci.*, 2019, **12**, 1542–1549.
189 L. Borchardt, D. Leistenschneider, J. Haase and M. Dvoyashkin, *Adv. Energy Mater.*, 2018, **8**, 1800892.
190 A. Eftekhari, *Energy Storage Mater.*, 2017, **9**, 47–69.
191 M. Watanabe, M. L. Thomas, S. Zhang, K. Ueno, T. Yasuda and K. Dokko, *Chem. Rev.*, 2017, **117**, 7190–7239.
192 D. Wang, Y. Wang, H. Liu, W. Xu and L. Xu, *Chem. Eng. J.*, 2018, **342**, 474–483.
193 J. Ewert, D. Weingarth, C. Denner, M. Friedrich, M. Zeiger, A. Schreiber, N. Jäckel, V. Presser and R. Kempe, *J. Mater. Chem. A*, 2015, **3**, 18906–18912.
194 P. Iamprasertkun, A. Krittayavathananon and M. Sawangphruk, *Carbon*, 2016, **102**, 455–461.
195 C. Kong, W. Qian, C. Zheng and W. Fei, *J. Mater. Chem. A*, 2015, **3**, 15858–15862.
196 Z. Song, H. Duan, L. Li, D. Zhu, T. Cao, Y. Lv, W. Xiong, Z. Wang, M. Liu and L. Gan, *Chem. Eng. J.*, 2019, **372**, 1216–1225.
197 C. Li, X. Zhang, K. Wang, X. Sun, G. Liu, J. Li, H. Tian, J. Li and Y. Ma, *Adv. Mater.*, 2017, **29**, 1604690.

Open Access Article. Published on 07 Adooleessa 2020. Downloaded on 01/02/2026 6:27:40 PM.
This article is licensed under a Creative Commons Attribution-NonCommercial 3.0 Unported Licence.

198 Q. D. Nguyen, J. Patra, C. Hsieh, J. Li, Q. Dong and J. K. Chang, *ChemSusChem*, 2019, **12**, 449–456.
199 R. Thangavel, A. G. Kannan, R. Ponraj, V. Thangavel, D.-W. Kim and Y.-S. Lee, *J. Power Sources*, 2018, **383**, 102–109.
200 J. Xu, N. Yuan, J. Razal, Y. Zheng, X. Zhou, J. Ding, K. Cho, S. H. Ge, R. Zhang, Y. Gogotsi and R. Baughman, *Energy Storage Mater.*, 2019, **22**, 323–329.
201 L. Zhang, K. Tsay, C. Bock and J. Zhang, *J. Power Sources*, 2016, **324**, 615–624.
202 J. Varela, K. Sankar, A. Hino, X. Lin, W. Chang, D. Coker and M. Grinstaff, *Chem. Commun.*, 2018, **54**, 5590–5593.
203 X. Wang, A. Y. Mehandzhiyski, B. Arstad, K. L. Van Aken, T. S. Mathis, A. Gallegos, Z. Tian, D. Ren, E. Sheridan and B. A. Grimes, *J. Am. Chem. Soc.*, 2017, **139**, 18681–18687.
204 C. Lian, K. Liu, K. L. Van Aken, Y. Gogotsi, D. J. Wesolowski, H. L. Liu, D. E. Jiang and J. Z. Wu, *ACS Energy Lett.*, 2016, **1**, 21–26.
205 A. Borenstein, R. Attias, O. Hanna, S. Luski, R. B. Kaner and D. Aurbach, *ChemElectroChem*, 2017, **4**, 2660–2668.
206 K. L. Van Aken, M. Beidaghi and Y. Gogotsi, *Angew. Chem., Int. Ed.*, 2015, **54**, 4806–4809.
207 L. Dagousset, G. Pognon, G. Nguyen, F. Vidal, S. Jus and P. H. Aubert, *J. Power Sources*, 2017, **359**, 242–249.
208 Y. Cho, C. Hwang, D. Cheong, Y. Kim and H. Song, *Adv. Mater.*, 2019, **31**, 1804909.
209 Z. Song, D. Zhu, L. Li, T. Chen, H. Duan, Z. Wang, Y. Lv, W. Xiong, M. Liu and L. Gan, *J. Mater. Chem. A*, 2019, **7**, 1177–1186.
210 Y. Gong, D. Li, C. Luo, Q. Fu and C. Pan, *Green Chem.*, 2017, **19**, 4132–4140.
211 Z. Song, D. Zhu, D. Xue, J. Yan, X. Chai, W. Xiong, Z. Wang, Y. Lv, T. Cao and M. Liu, *ACS Appl. Energy Mater.*, 2018, **1**, 4293–4303.
212 Y. Ahn, B. Kim, J. Ko, D. You, Z. Yin, H. Kim, D. Shin, S. Cho, J. Yoo and Y. S. Kim, *J. Mater. Chem. A*, 2016, **4**, 4386–4391.
213 X. Peng, H. Liu, Q. Yin, J. Wu, P. Chen, G. Zhang, G. Liu, C. Wu and Y. Xie, *Nat. Commun.*, 2016, **7**, 11782.
214 X. Zhang, M. Kar, T. Mendes, Y. Wu and D. MacFarlane, *Adv. Energy Mater.*, 2018, **8**, 1702702.
215 X. Chen, X. Liu, A. Pandian, K. Lou, F. Delnick and N. Dudney, *ACS Energy Lett.*, 2019, **4**, 1080–1085.
216 V. Vijayakumar, B. Anothumakkool, A. T. A. Torris, S. B. Nair, M. V. Badiger and S. Kurungot, *J. Mater. Chem. A*, 2017, **5**, 8461–8476.
217 Y. Huang, M. Zhong, Y. Huang, M. Zhu, Z. Pei, Z. Wang, Q. Xue, X. Xie and C. Zhi, *Nat. Commun.*, 2015, **6**, 10310.

 This journal is © The Royal Society of Chemistry 2020